RESEARCH MEMORANDUM

AN INVESTIGATION OF SCREENS FOR REMOVING DISTORTIONS IN DUCTED FLOWS AT HIGH SUBSONIC SPEEDS

By Charles C. Wood and Gerald Knip, Jr.

Langley Aeronautical Laboratory
Langley Field, Va.

NATIONAL ADVISORY COMMITTEE
FOR AERONAUTICS

WASHINGTON
September 26, 1957

NATIONAL ADVISORY COMMITTEE FOR AERONAUTICS

RESEARCH MEMORANDUM

AN INVESTIGATION OF SCREENS FOR REMOVING DISTORTIONS IN DUCTED FLOWS AT HIGH SUBSONIC SPEEDS

By Charles C. Wood and Gerald Knip, Jr.

SUMMARY

In order to aid in the research concerning the problem of obtaining uniform flow in ducts, an investigation of resistance screens was conducted for the purposes of (1) providing systematic data for the Mach number range from 0.20 to 0.65 on the flow smoothing effect of screens for various types of flow nonuniformities together with the consequent cost in total-pressure loss, (2) determining screen design methods for reducing the total-pressure losses required to accomplish various degrees of flow smoothing, and (3) summarizing the data in the literature on screen total-pressure losses in a convenient form suitable for engineering studies. The experimental data were obtained in a directly connected rectangular duct in which the nonuniform flow distributions were produced by spoilers located upstream from the screens.

The new screen designs investigated consisted of several different screen shapes with the elements set at oblique angles (swept) to the flow. The screen variables investigated were solidity, angle of sweep, rod diameter, rod cross-sectional shape, and screen plan forms. Design charts for predicting screen total-pressure losses, changes in velocity distribution, downstream Mach numbers, drag coefficient, and choking Mach number are presented. For equivalent improvements in flow uniformity at a given duct Mach number, swept screens reduced the total-pressure losses as much as 45 percent in comparison with those for straight screens. The loss coefficients of swept screens were correlated with those for straight screens by assigning an effective blocked area ratio to the swept screens which is equal to the geometric projected blocked area ratio multiplied by the cosine of the sweep angle.

A limited number of tests were conducted with screens installed in a rectangular diffuser.

INTRODUCTION

The requirements for the uniformity of ducted flows in current aircraft and in other applications have resulted in a demand for duct design methods whereby highly uniform flows may be obtained and in a demand for techniques for reducing flow nonuniformities once they develop. Inasmuch as flow uniformity is influenced by many factors - for instance, the pressure gradient, shock-boundary-layer interaction, turns which the flow must negotiate, changes in duct cross-sectional shape, and other factors, some sort of flow control device frequently represents the most expedient solution. A resistance screen is one such device and is the subject of the investigation reported herein.

Resistance screens located perpendicular to the flow have been investigated on numerous occasions, and the available literature is listed in references 1 to 7. References 1 and 2 contain comprehensive data on screen pressure-loss coefficients. The data of reference 1 cover the Mach number range of current interest from 0.2 to the choking Mach number of the screen; the data of reference 2 are for Mach numbers below 0.1. The investigations of both references 1 and 2 correspond to uniform flow with negligible boundary-layer thickness upstream from the screens. Reference 3 summarizes screen literature published prior to 1950, and references 4 and 5 compare data at low speeds with theoretical relations derived for the purpose of predicting flow distributions downstream of screens. Reference 6 reports data on the flow development in a diffuser at low speed in which single or multiscreen configurations were located at or upstream from the diffuser exit. Reference 7 is one of several papers reporting the effects of screens on stream turbulence. No data for high subsonic Mach numbers are available which systematically evaluate the flow smoothing effect of screens for various types of flow nonuniformities and which evaluate the consequent cost in total-pressure loss.

The purposes of the present investigation are to provide such data, to determine screen design methods for reducing the total-pressure losses required to accomplish various degrees of flow smoothing, and to summarize the data in the literature on screen losses in a convenient form suitable for engineering use. The new screen designs investigated consisted of several different screen shapes with the elements set at oblique angles (swept) to the flow. Most of the data presented herein were obtained from tests made in a directly connected duct in which flow nonuniformities similar to the various types obtained in airplane inlet ducting were simulated through the use of spoiler configurations located upstream from the screens. The test section was rectangular in cross section with an aspect ratio of 2.86; the test-section Mach numbers ranged from 0.20 to approximately 0.65 and the maximum Reynolds number based on a rod diameter of 1/8 inch was approximately 33,000. The upstream flow distortions were

produced in planes parallel to the narrow dimension of the test section, and all the elements of the screens were parallel to the same dimension. A limited number of data were obtained with screens installed in a rectangular diffuser to determine the effects of the screens on the diffuser total-pressure losses.

SYMBOLS

A	duct cross-sectional area
b	space between end rod of screen and brace plate (see figs. 4 and 6)
c	space between individual rods of screen (see figs. 4 and 6)
d	screen-wire diameter
D	total drag force on screen
f	free area ratio of screen, $\frac{\text{(Duct cross-sectional area) - (Projected screen area)}}{\text{Duct cross-sectional area}}$
$1 - f$	screen solidity ratio
$(1 - f)_e$	effective screen solidity ratio, $(1 - f)\cos \psi$
h	height of duct, larger dimension (see fig. 6)
H	total pressure
ΔH	total-pressure loss
m	mass flow
M	Mach number
M_s	Mach number just upstream from normal shock
p	static pressure
q	incompressible dynamic pressure
q_c	compressible dynamic pressure, $H - p$

[redacted]

u	local stream velocity
U	maximum velocity in a profile at a given duct station
w	duct width, smaller dimension (see fig. 6)
x	distance from wall in same plane as h or w (see fig. 1)
γ	ratio of specific heats
δ	boundary-layer thickness
δ^*/w	displacement thickness, $\int_0^{\delta/w}\left(1 - \frac{u}{U}\right)d\left(\frac{x}{w}\right)$
ψ	angle of sweep of screen (see figs. 4 and 6)
$C_D(1 - f)$	drag coefficient based on duct area, D/qA
C_D	drag coefficient based on projected screen area, $\frac{D}{qA(1 - f)}$

Subscripts:

1	reference station
2	station in vicinity of screens
3, 4, 5	survey stations downstream of screen location (see figs. 1 and 3)
A	wall A (see figs. 1, 2, and 3)
B	wall B (see figs. 1, 2, and 3)

APPARATUS AND PROCEDURE

GENERAL APPARATUS

Two individual test setups were used in this investigation: one having a straight rectangular channel as the test section and the other, a rectangular two-dimensional diffuser. The majority of the tests were conducted with the rectangular-channel test section; the general setup (fig. 1) consisted of a 40-inch-diameter settling chamber with screens for damping the flow, an inlet bell, two rectangular-channel ducts

(7 by 20 inches in cross section), a venturi tube, and an exit diffuser. The screen configurations were inserted between mating flanges of the two rectangular ducts; the screen support members were flush with the duct surfaces and the joint was sealed. Spoilers were located upstream from the screens to produce the desired nonuniform flow distributions. (See fig. 2.) The spoilers in each case extended the full height of the duct.

The effect of a screen on the performance of a diffuser was studied briefly by means of the setup shown in figure 3. This setup consisted of a 30-inch-diameter settling chamber, an inlet bell, a two-dimensional diffuser, a square straight section, and an exit diffuser. The diffuser test section was a conventional straight walled diffuser of constant height with an area ratio of 2:1 and with the side walls expanding at 3.1°. In most instances, the screens were located between the exit flange of the diffuser and the flange of the square straight section. A single-screen configuration was tested in the diffuser upstream from the exit. Desired flow distributions upstream from the screens were produced by operating with the diffuser inlet choked and with a standing normal shock in the diffuser.

SCREEN MODELS

During this investigation, the 19 screen models listed in table I were tested. The screen models were constructed of equally spaced parallel rods of small diameter whose axes were in the plane of the major flow distortion (narrow dimension of test section). Typical screen models are shown in figures 4, 5, and 6. The screen variables investigated were screen solidity, rod diameter, rod cross section, sweep angle, and screen plan form. The ranges for these variables are shown in the table. A majority of the tests were conducted with Λ-shaped screens having 1/8-inch-diameter rods and sweep angles equal to or less than 45°.

INSTRUMENTATION

Instrumentation for the rectangular-channel configuration is shown in figure 1. A reference total-pressure tube and a thermocouple were located in the 40-inch settling chamber. Static-pressure orifices were located on the center line of each of the four walls at stations 1, 2, 3, 4, and 5. Total-pressure traverses were made at stations 2, 3, 4, and 5 as shown in figure 1. Total-pressure traverses at stations 3 and 4 in the plane perpendicular to the narrow tunnel dimension were made midway between the duct center line and outer wall B in order to avoid the wake of the screen strut. Wall static pressures were recorded by photographing a multitube manometer board to which the pressure orifices were connected.

[redacted]

All data obtained from total-pressure traverses were recorded by commercial transducer pressure cells used in conjunction with electronic data plotters which limited the frequency response to 10 cycles or less and gave a continuous plot of the pressure loss from the reference tube to the survey position. In all cases the data were obtained to within 0.05 inch of each wall.

Similar instrumentation was used for the diffuser setup (fig. 3). The total-pressure reference tube and thermocouple were again located in the settling chamber (30-inch diameter) and static-pressure orifices were located on the center line of each wall at stations 1, 2, 3, 4, and 5. Additional static orifices were located at 1-inch intervals along the center line of wall B for the entire length of the diffuser. Total-pressure traverses were made on the vertical and horizontal center lines at station 2 but only on the horizontal center lines at stations 3 and 4.

TEST PROCEDURE

The investigation conducted with the rectangular-duct configuration was initiated by obtaining total-pressure traverses at station 2 in the absence of screens and spoilers for a duct Mach number range from approximately 0.2 to 0.7. These measurements were then repeated after the installation of several spoiler configurations in the upstream duct until the three desired flow distributions were obtained. The three spoiler configurations used to produce the three different flow distributions are shown in figure 2. After these preliminary traverses at station 2 were completed, the rakes were removed and traverses were made at stations 3, 4, and 5 for the three spoiler configurations over the same general speed range. Measurements made at stations 3 and 4 served as the basis for comparing traverses made with screens; whereas, measurements made at station 5 were used to calibrate the venturi tube for total pressure for use in determining the screen total-pressure-loss coefficient. The rakes at station 5 were then removed, screens were installed, and tests were conducted with the three test configurations over the given speed range.

For the diffuser investigation, total-pressure traverses were made at stations 2, 3, and 4, and the reading of the static-pressure wall orifices was recorded in the absence of screens for a variety of diffuser flow conditions. Changes in diffuser flow condition were produced by choking the diffuser throat and by regulating the location of the normal shock in the diffuser by means of a valve. Screens were then installed and tests were repeated for the normal shock locations desired.

PERFORMANCE PARAMETERS

Screens tested in this investigation were compared on the basis of the following performance parameters: (1) total-pressure-loss coefficient, (2) the velocity distribution at station 4, and (3) the displacement thickness corresponding to the station 4 velocity distributions. The total-pressure-loss coefficient of a screen is defined as the ratio of the total-pressure loss due to the screen to the one-dimensional, compressible, dynamic pressure at station 2. This loss due to the screen is defined as the increase in the total-pressure loss from stations 1 to 5 produced by the installation of the screen. The total pressure at station 5 was calculated from one-dimensional relations by the use of the static-pressure measurements at station 5 and the mass flow measured in the inlet bell. Venturi-tube calibration data indicated that total-pressure values so calculated were essentially equal to mass-weighted values obtained from surveys. The compressible dynamic pressure in the denominator of the screen total-pressure-loss coefficient was determined from the measured mass flow and the calculated total pressure at station 2, which was obtained from the total pressure at station 5 without screens installed and the estimated total-pressure loss between stations 2 and 5 due to friction. Velocity distributions are presented as the ratio of the local to the maximum velocity occurring in the same cross-sectional plane. Values of displacement thickness presented were determined according to the two-dimensional incompressible definition given previously in the list of symbols. The Mach number M_2 which is used as a correlating parameter is a calculated Mach number obtained in a manner similar to the total pressure H_2 described previously.

RESULTS AND DISCUSSION

RECTANGULAR-CHANNEL INVESTIGATION

Duct Calibration

Velocity distribution.- Velocity distributions for test configurations I, II, and III obtained from total-pressure surveys made at the positions given in figure 1 are presented in figure 7 for the case without screens. Spoilers installed on the side walls were used to produce in the horizontal plane (narrow tunnel dimension) the velocity distributions desired while the velocity distributions in the vertical plane were allowed to develop without interference. The distributions presented were not significantly affected by the Mach number of the flow. For test configuration I the flow at station 2 is nonsymmetrical with the high-velocity-air core located at the 25-percent-area location. The minimum

[redacted]

velocity ratio is adjacent to wall A and is about 0.4. For test configuration II the flow at station 2 is symmetrical with the high-velocity-air core at the duct center. The boundary-layer thickness at each wall is 30 percent of the duct width, and the minimum velocity ratio is adjacent to wall B and is less than 0.4. For test configuration III the flow at station 2 is symmetrical with low velocity air at the duct center and high velocity air on each side between the duct center and the walls. The boundary-layer thickness is approximately 10 percent of the duct width and the velocity ratio adjacent to both walls is about 0.7. The velocity distributions at station 4 indicate that the flow in the vertical plane is reasonably uniform for all configurations and that the boundary-layer thickness is approximately 10 percent of the duct height. Traverses in the horizontal plane at stations 3 and 4 show that the flow became somewhat more uniform as it progressed downstream from station 2, as would be expected because of natural mixing in the constant-area channel. For test configuration I the measurements at station 5 show that the flow is relatively uniform because of the flow acceleration through the throat of the venturi tube. Uniformity of the flow in the venturi-tube throat permits the total pressure at station 5 to be calculated accurately in the manner described previously.

Total-pressure-loss coefficients.- The loss of total pressure between stations 1 and 5 expressed as a coefficient $\frac{\Delta H_{1-5}}{q_{c,2}}$ is presented in figure 8 as a function of Mach number M_2 for the three test configurations in the absence of screens. These data, as previously described, were subtracted from values obtained with the screens in place to determine the screen loss coefficients. The magnitude of the coefficients and the trend with Mach number appear to be reasonable for the duct and spoiler configurations involved.

Basic Screen Data

Configuration I.- Velocity distributions in both the horizontal and vertical planes at stations 3 and 4 for a screen with no sweep (straight) and a Λ-shaped screen with 45° sweep angle are presented in figure 9. Velocity distributions in the vertical direction were located in the plane midway between the model center line and wall B where the duct velocity was near the maximum. The sizeable irregularities apparent in the velocity distributions at station 3 result from wakes of the individual rods from which the screens were made. These wakes were dissipated between stations 3 and 4; consequently, comparisons of screen performance herein are based on measurements at station 4. The smaller wakes noted for swept screens are due in part to the well-known beneficial effect of sweep on drag; however, the greater distance between the rods producing the wakes and the traverse rake for the swept screen also would allow the wakes to disperse to a greater extent than those for the straight screen.

Velocity distributions determined from measurements in the horizontal plane at station 4 for all screens tested with test configuration I are presented in figure 10. In general, the effect of screens was to raise the relative velocity on the side of the model center line corresponding to the major velocity deficiency. The magnitude of relative velocity increase was affected by screen solidity, inlet Mach number to the screen, angle of screen sweep, screen plan form, rod diameter, and the cross-sectional shape of the screen members. Flow distributions on the side opposite the major velocity deficiency (wall A) were virtually unaffected by the various screens tested.

The displacement thickness δ^*/w determined from velocity profiles at station 4 is presented in figure 11 as a function of the Mach number at station 2. This parameter δ^*/w is an index to flow uniformity and is used in later sections to analyze the effects of various screen variables. The displacement thickness for test configuration I is defined as that present on the A wall of the duct, the side of the major flow distortion. The data of figure 11 show that the effect of Mach number is to reduce the displacement thickness for almost all screens. It is obvious that a true evaluation of this effect or any other variable represented cannot be accomplished without simultaneous consideration of the variation of the screen loss coefficient. Such an analysis will be made in a later section in which the basic data of figure 11 are utilized. It should be noted that with no screen (fig. 11(a)), the displacement thickness was approximately constant with Mach number and corresponds to about twice the value for a fully developed, symmetrical turbulent boundary layer with a 1/7-power-profile variation.

The total-pressure-loss coefficient of various screens tested with test configuration I are presented in figure 12 as a function of the duct Mach number at station 2. The loss coefficient increased with Mach number in all cases except for screens with 75° sweep. The effect of increasing loss with increasing Mach number has been noted previously in the literature (i.e., ref. 1).

Configurations II and III.- Velocity distributions based on measurements obtained in the horizontal plane at station 4 for the various screens tested with test configurations II and III are presented in figures 13 and 14, respectively. Irregularities in the velocity profile near the duct center line for the high-speed condition for test configuration II and no screens are the result of shocks which formed when the flow choked in the plane of the spoilers.

The large differences in the shape of the velocity distributions for the M- and W-screens shown in figure 13(b) are of considerable interest. The mechanics of swept-screen operation are described in reference 3. Briefly, it may be stated that a change in flow direction occurs through inclined screens so that the upstream flow turns in a

[redacted]

normal direction into the plane of the screen, which results in a shift of the flow transversely. It is desired to shift the flow of configuration II from the duct center towards the duct walls. According to the preceding theory the Λ-shaped screens would accomplish the reverse; consequently, the screens should have been reversed in direction to form a V-shape. However, reversing the screen would have located the screen apex close to the survey station which would have been undesirable because of wakes in the survey plane. This undesirable feature was overcome by adding highly swept legs that gave an M-shape to the screen and produced the correct turn in direction for the flow of configuration II and, yet, the screen remained a significant distance upstream from the survey station. Since this screen could be oriented with the center apex pointing either upstream or downstream (W and M) and yet occupy the same approximate duct location, it was ideal for the purpose of verifying the theory noted. When the screen is oriented upstream (W-screen) the requirements for test configuration III are satisfied since the flow is directed into the velocity deficiency region at the duct center.

The M-shaped screen produced for test configuration II (fig. 13(b)) velocity distributions which contained a velocity deficiency region of significant size at the duct center. The velocity deficiency region was reduced in size by eliminating the screen support strut. The velocity distribution obtained suggests that by shaping the center V element correctly the velocity deficiency could be reduced further and the peak velocity regions shifted toward the walls. Tests conducted with configuration II with the M-screen reversed in direction, W-screen, produced an unfavorable change in the velocity distribution as would be expected. A peak velocity occurred at the center line; the velocity decreased rapidly in a region extending over 30 percent of the duct width on both sides of the center line and then varied somewhat irregularly in the remaining 20 percent of the duct width adjacent to the duct walls.

The M-screen enlarged the velocity deficiency region at the duct center for test configutation III (fig. 14(b)) and was actually detrimental to the distributions. Tests conducted with the screen in the W-configuration, which is correct according to the theory, produced a significantly different distribution; the velocity deficiency region remained and extended over 60 percent of the duct width. Velocity ratios in the region were practically constant at a value of approximately 0.87. Velocity distributions produced by both the M-screen and W-screen are inferior to the velocity distribution with no screen (fig. 14(a)). The velocity distribution obtained with the W-screen suggests that a more uniform distribution could have been obtained by shaping the screen to provide more sweep at the duct center line and less sweep in regions from 5 percent to 10 percent of the width from the walls. Such modifications would tend to reduce the total-pressure losses on the center line and to increase them at the velocity peaks. The test results for the M-screen

and W-screen for configuration II and the M-screen for configuration III support the theory of reference 3, and the results with the W-screen and configuration III do not necessarily violate it.

Figures 15 and 16 present for configurations II and III, respectively, the displacement thickness δ^*/w as a function of M_2 for the screens tested. The displacement thickness for test configuration II is the sum of the integrated velocity deficiency areas adjacent to walls A and B; whereas, for test configuration III the displacement thickness is determined from the integrated velocity deficiency area near the duct center. The velocity deficiency area adjacent to the walls was not considered in the case of configuration III. The displacement thickness for configuration II with no screens is approximately equal to that for a fully developed symmetrical turbulent boundary layer with a 1/7-power profile.

The total-pressure-loss coefficients for the various screens tested with test configurations II and III are presented as a function of M_2 in figures 17 and 18, respectively.

Data Analysis for Configuration I

Screen total-pressure-loss coefficient.- Total-pressure-loss data for straight screens with solidities ranging from 0.15 to 0.40 are presented in figure 19 as a function of duct Mach number immediately upstream from the screen. The curves presented are faired curves determined from cross plots of the original data presented in reference 1, and the data presented herein for test configuration I. Data in reference 1 were obtained from tests conducted in a circular duct 9 inches in diameter in which a uniform flow with negligible boundary layer was present at the screen location. Screens were constructed of commercial wire mesh having a maximum wire diameter of 0.041 inch. These data are the most comprehensive in existence on basic screen characteristics for the Mach number range of current interest. Theoretical values of screen loss coefficient for constant values of drag coefficient and Mach number downstream are also presented in this figure. The theoretical loss coefficient and the downstream Mach number are determined by the duct Mach number upstream of the screen and the drag coefficient $C_D(1 - f)$. The equations required for the calculation of these curves are developed in the appendix. The Mach number at station 4 M_4 is of interest because it permits the determination of the increase in Mach number across the screen due to the screen total-pressure loss. The drag coefficient is of interest to designers since it permits the total load on the screen to be calculated rapidly. The value of M_2 for which a Mach number of 1.0 exists in the plane of the screen is designated the choking Mach number and is also plotted in figure 19. The choking Mach numbers for the screens presented in reference 1 are larger than those determined theoretically by one-dimensional

relations and the geometric solidity ratios. A possible explanation for this difference is that the solidity based on projected area, which is the usual procedure, is not the true solidity, but is slightly less because of the woven nature of the screen. The choking Mach number lines in figure 19 and subsequent figures is the average of values taken from reference 1 and values determined by one-dimensional relations. Values determined by this procedure are in error by only small amounts for either woven screen or screen made up of all parallel elements.

The theoretical curves of total-pressure-loss coefficient for constant values of drag coefficient $C_D(1 - f)$ rise slowly and steadily with increasing Mach number. The experimental curves for constant values of solidity $1 - f$ increase much more rapidly with Mach number, especially near the choking line and at the higher solidities. The differences between the slopes of the two sets of curves are indicative of the rapid increase with Mach number of the drag coefficient based on the projected area of the screen elements C_D. This effect is not only due to the well-known effect of compressibility on drag coefficient but also is due to the interference effects between individual members composing the screen.

In order to illustrate the accuracy of the data and the fairings, the data of reference 1 and configuration I used in preparing figure 19 are presented in figure 20 together with the resulting faired curves. The loss-coefficient data for the straight screens of configuration I having all parallel rods agree with the data curves of reference 1 for woven mesh screens within the accuracy of the data of reference 1. A maximum inaccuracy of about 0.15 in terms of $\Delta H/q_{c,2}$ occurs for the reference 1 curves at a solidity of about 0.37 and for the configuration I data at a solidity of about 0.30. Figure 21 is similar to figure 20 but covers a wider range of solidity from 0.15 to 0.62. The faired curves in figure 21 for screen solidities greater than 0.35 were based solely on data from reference 1 since the limiting solidity for current investigation was 0.302. Data obtained with configuration I have been omitted from figure 21 for the sake of clarity. The data from reference 2 which were obtained at low Mach numbers and low Reynolds numbers are included for comparison. The experimental setup used to obtain the low Mach number data presented in reference 2 was similar to that used to obtain the data reported in reference 1 and consisted of a circular-tube test section, uniform flow upstream from the screen, and wire-mesh-type screens. The Reynolds number of the reference 2 data, based on wire diameter, was considerably below 1,000 and the flow was largely laminar. Reference 2 data presented in figure 21 and the data from reference 1 agree for screen solidities below 0.328; data for screen solidities greater than 0.496 vary erratically and do not agree with those of reference 1.

The screen total-pressure-loss-coefficient data of figure 12 for configuration I are presented in figure 22 in terms of the drag coefficient $C_D(1 - f)$ as a function of Mach number M_2. Faired curves for straight screens derived from figure 19 are included to facilitate comparison. The figure could have been presented in terms of loss coefficient; however, drag-coefficient curves are somewhat easier to fair since the slope is less than that for total-pressure-loss-coefficient curves. Numerical values of loss coefficient and drag coefficient are equal at incompressible speeds as shown in figure 19.

The very large effect of angle of sweep on the drag and, thus, on the loss coefficient is very apparent in figure 22. Sweep angles as high as 60° or 75° produced only a fraction of the drag of the straight screen. An inspection of the figure indicates that the swept-screen curves appear to belong to the same family of curves as the faired curves for the straight screens. This observation leads to the conclusion that the swept screens should be identified with an effective blocked area ratio determinable from the positions which the swept screens occupy in the family of straight-screen curves. The effective blocked area ratio $(1 - f)_e$ was found to correspond closely to the product $(1 - f)\cos \psi$, and these values are given opposite each data curve. When the swept-screen curves are considered to have the effective blocked area ratio $(1 - f)_e$, they fit the straight-screen family of curves as accurately as the straight-screen data of configuration I, which was used in part in obtaining the faired curves. The exceptions to this conclusion are the data for screen shape II and the streamline rods, which would not be expected to conform. The concept of effective blocked area ratio permits the straight-screen data of figures 19 and 21 to be used in determining the loss characteristics of swept screens with all parallel elements. Whether swept screens with square or rectangular mesh also fit this concept is not known.

The loss-coefficient curve for the M-shaped screen given in figure 12(b) is about the same as that for the 1/16-inch diameter rods. A weighted value of effective blocked area ratio $(1 - f)_e$ for the M-screen was calculated to be 0.175 by considering two-sevenths of the screen to be at a sweep angle of 75° and five-sevenths of the screen to be at a sweep angle of 45° (see fig. 5). In figure 22 it is shown that a curve with a value of $(1 - f)_e$ of 0.175 in the vicinity of the 1/16-inch-rod curve would fit the straight-screen data accurately.

The data of figure 22 also show that the use of streamlined rods reduced the drag to about one-half of that for circular rods of the same sweep angle. Rounding the apex of the Λ-screen, screen shape II, increased the drag about 20 percent at $M_2 = 0.25$ and 45 percent at $M_2 = 0.50$. There is some evidence that increasing the rod diameter

increased the drag; however, the range of rod diameters included is not sufficient to be conclusive. The data for high sweep angles and for streamline rods indicate that inlet screens designed to protect the engine from foreign objects may be designed to have very low drag.

References in the literature (i.e., ref. 3) have proposed that the loss coefficient of a swept screen is directly proportional to the cosine of the sweep angle raised to a power. The preceding discussion indicates that swept screens can be treated as straight screens provided an effective blockage ratio is utilized. Since the loss coefficient of straight screens is a function of blockage ratio and Mach number, it follows that the loss coefficient of swept screens is also a function of these variables in addition to the sweep angle. This fact is illustrated in figure 23 where the ratio of the swept-screen loss coefficient to the straight-screen loss coefficient is expressed as a function of sweep angle for several Mach numbers M_2 and two blockage ratios $(1 - f)$ for the Λ-shaped screens with 1/8-inch-diameter rods. Curves of $\cos^3\psi$ and $\cos\psi$ are given for comparison. It is apparent that the swept-screen loss coefficient is not a simple function of $\cos\psi$.

Effect of screens on flow uniformity.- In the case of configuration I the displacement thickness at station 4 on the side of the duct where the velocity deficiency was located was selected as a measure of flow nonuniformity. It became apparent early in the investigation that reductions in displacement thickness were generally coincident with proportionate increases in total-pressure-loss coefficient and that both variables had to be considered simultaneously in comparing screen performances. The presentation in figure 24 accomplishes this comparison for the screens tested with configuration I and consists of the loss coefficient and drag expressed as a function of the percent change in displacement thickness for constant values of Mach number M_2 and sweep angle ψ. The shaped screens with angles of sweep from 15° to 45° produced larger changes in δ^*/w per unit loss coefficient than the straight screens; whereas, swept screens with angles of sweep of 60° and 75° produced smaller changes in δ^*/w than the straight screens. The 45° swept screen produced the highest performance at all Mach numbers; for instance, at a Mach number of 0.55 the 45° screen required only about three-quarters of the loss of the straight screen for a 43-percent reduction in δ^*/w.

The Λ-shaped screen is probably not the optimum screen shape for the velocity distribution of configuration I. If it is assumed that the flow turns normal to the screen plane and, thus, shifts the distribution, the leg of the Λ-screen on the side with the velocity deficiency (A wall) is alined incorrectly. The effectiveness of the screen probably could have been improved by extending the other leg of the screen (on the B wall) past the middle of the duct to some point near the A wall and then joining

that leg to the A wall with a highly swept member. Such a screen would resemble the right half of the M-screen.

Modifying the cross section of the screen rods from a circular to a streamline shape resulted in a less effective screen, as shown by figure 24. More total-pressure loss was required by the streamline rods for a given reduction in δ^*/w. In order to avoid complicating the presentation, the data for the M-screen and screen shape II are not presented in figure 24; however, the M-screen increased the displacement thickness, as shown in figure 11(b), and screen shape II was less effective than shape I because of its higher loss characteristics.

Screen efficiency.- Screens cause a nonuniform flow distribution to become more uniform primarily by producing total-pressure losses. Unfortunately, total-pressure losses occur across the entire width of the duct instead of just in the high total-pressure regions. However, some screen designs may produce a larger proportion of the overall total-pressure loss in the desired region and, therefore, would be considered more efficient. Figure 25 illustrates this concept in more detail. Total-pressure distributions at stations 2 and 4 are presented for straight screens and Λ-shaped screens with 45° sweep and several screen solidities. The distribution at station 4 is presented twice on each figure. The lowest curve (curve C) represents the measured values, and the middle curve (curve B) is the lower one (curve C) displaced upward a sufficient amount to be tangent to the distribution at station 2 (curve A) near one or both walls. The area bounded by curves A and B represents the total-pressure loss which was expended usefully to produce a more uniform distribution. The area bounded by curves B and C represents a wasted total-pressure loss. The ratio of area $\overline{AB}$ to area $\overline{AC}$ may be considered an efficiency. The efficiency so defined is given in figure 26 for the screens with sweep angles of 0° and 45°. The efficiency decreases with increasing solidity for both straight and Λ-shaped screens, and the efficiency of the swept screens is approximately 17 percent greater than that for the straight screens. The efficiencies range from about 45 percent to 60 percent, which suggests that the Λ-shaped screen is not an optimum shape.

Data Analysis for Configurations II and III

Screen total-pressure-loss coefficient.- The drag coefficients for several screens tested with configurations II and III are presented in figure 27 together with data curves for the same screens for configuration I for comparison. The drag coefficients for configurations I and II were essentially equal for a given screen and Mach number, as shown in the upper half of figure 27. Since the total-pressure loss can be determined directly from the drag coefficient and duct Mach number, the loss coefficients for test configurations I and II also would be equal for a particular screen. In the lower half of figure 27 the drag coefficients

for test configuration III (total-pressure deficiency on model center line) are indicated to be appreciably less than those for test configuration I up to a Mach number of about 0.5, where the two sets of data coincide approximately.

Effect of screens on flow uniformity.- The total-pressure loss and drag coefficients for configurations II and III are presented as functions of the percent change in displacement thickness in figures 28 and 29, respectively. Dashed curves for configuration I are given for comparison. For configuration II (fig. 28) for straight screens the change in displacement thickness per unit loss coefficient was much less than for configuration I at Mach numbers M_2 of 0.25 and 0.35; at $M_2 = 0.45$ the changes in displacement thickness for configurations I and II were equal. The Λ-shaped screens with 45° sweep had less desirable performance than the straight screens, which would be expected since the screen was oriented (alined) in such a manner that the flow would be shifted toward the duct center line instead of toward the walls. The W-screen in some cases increased the displacement thickness, and its alinement also was incorrect. The M-shaped screen, with or without the strut, produced the largest reductions in displacement thickness per unit loss coefficient of any screen tested, and its alinement was in the correct manner. For instance, at a Mach number of 0.45 and for a 56-percent reduction in δ^*/w the M-screen with no strut had only 55 percent of the loss coefficient of the straight screen.

For configuration III (fig. 29) the performances of the straight screens were the highest of any tested. The W-shaped screen, which was alined correctly, did not improve the performance for reasons discussed in a previous section.

DIFFUSER INVESTIGATION

Velocity Distributions

Velocity distributions obtained from surveys at station 4 are presented in figure 30 for two different flow conditions: one with the diffuser choked and no normal shock and one with a normal shock at a Mach number of 1.43. With no screen and no normal shock (shock Mach number of 1.0) the flow was symmetrical and had a boundary-layer thickness on each wall of about 30 percent of the duct width. The velocity ratio at the walls was about 0.5. For a shock Mach number of 1.43 and with no screens the flow was badly distorted but not separated at the point of measurement. Measurements not presented here, which were made 12 inches upstream from the diffuser exit, indicated appreciable separation adjacent to wall B.

All screens tested improved the flow uniformity for both test conditions; however, the most uniform and symmetrical flow was obtained with the straight screen located 15 inches upstream from the diffuser exit (fig. 30(a)). Velocity ratios near the wall were about 0.7 in this case. Measurements made 12 inches upstream from the diffuser exit indicated no separation.

With either straight or swept screens installed at the diffuser exit the flow was less symmetrical and less uniform than for the straight screen installed upstream. Measurements upstream in the diffuser showed that separation was not eliminated by any of the screen installations at the exit for the case with a shock Mach number of 1.43. The two swept-screen installations at the exit, however, caused the flow separation to shift from wall B to wall A. The data show that the ability of a screen to eliminate or to reduce flow-separation regions in the diffuser depends strongly on the screen location.

Total-Pressure Loss

The total-pressure loss of the diffuser with no screen and with the straight screen located at the diffuser exit and upstream in the diffuser is presented in figure 31 as a function of the shock Mach number in the diffuser. The overall loss measured with no screen may be considered to consist of three parts: the one-dimensional normal-shock loss, the basic diffuser loss that would be obtained in the absence of a shock, and the difference between the overall measured loss and the sum of the first two. This difference is normally referred to as the loss resulting from the interaction of the shock wave and the boundary layer. Figure 31 shows that the interaction loss is the major component of the overall loss over a large portion of the range of shock Mach numbers and that it amounts to about 10 percent of the total pressure at a value of M_s of 1.45. If the screens improved the flow in the diffuser, the interaction loss probably would be reduced. The total-pressure losses with the screens in either location were higher than those with no screen, and the screen which was installed upstream from the exit produced higher losses than the exit installation because of the higher velocity level upstream.

It is of interest to determine whether the additional losses due to screens correspond to the screen losses measured in the rectangular-channel investigation. The analysis presented in figure 32 was prepared for this purpose. The change in diffuser total-pressure-loss coefficient due to the screen installation is presented as a function of the Mach number immediately upstream from the screen. The denominator of the loss coefficient is the compressible dynamic pressure just upstream from the screens. The curve for the loss-coefficient values obtained in the channel tests of the same screen is also included. With the screen installed

at either the diffuser exit or in the diffuser 15 inches upstream from the diffuser exit, the additional diffuser losses due to the screen were approximately equal to the screen loss measured in the channel tests and indicate that the screen loss added directly to the diffuser loss. More information obtained in an investigation at low speed on the placing of a series of screens in strategic locations in diffusers is available in reference 6.

CONCLUSIONS

An investigation was conducted to determine the effectiveness of screens as devices for removing flow distortions at duct Mach numbers up to 0.65 and to determine the consequent total-pressure losses. The screens consisted of parallel and equally spaced rods whose axes were set perpendicular to the flow direction (straight screens) as well as at oblique angles to the flow direction (swept screens) for several different configurations (Λ-shape, W-shape, and M-shape). The investigation was conducted in a 7- by 20-inch rectangular duct in which the flow distortions and the axes of the screen elements were located in planes parallel to the 7-inch dimension. A limited number of tests were conducted with screens installed in a rectangular two-dimensional diffuser. From the results of this investigation the following conclusions were indicated:

1. The reduction in flow distortion and the total-pressure loss produced by either the straight or swept screen increased with increasing screen solidity and with increase in the duct Mach number.

2. The flow distribution upstream from the screens did not affect the screen total-pressure-loss coefficients except for the case where a region of velocity deficiency in the form of a wake existed in the middle of the stream. The loss coefficients in this case were appreciably smaller at Mach numbers less than 0.5.

3. The total-pressure-loss-coefficient data for swept screens correlated with the straight-screen data when the swept screens were considered to have an effective blocked area ratio equal to the geometric projected blocked area ratio multiplied by the cosine of the sweep angle.

4. Swept screens tend to turn the flow perpendicular to the plane of the screen and, thus, to alter the flow distribution favorably or unfavorably according to the direction of sweep and the location of the high mass-flow regions.

5. For equivalent improvements in the flow uniformity the use of a swept-screen configuration which takes advantage of the inherent turning

action may reduce the total-pressure losses as much as 45 percent in comparison with those for a straight screen.

6. The effectiveness of screens for reducing the extent of or eliminating regions of flow separation in a diffuser caused by shock-wave—boundary-layer interaction is significantly improved by locating the screen in the vicinity of the initial line of flow separation.

Langley Aeronautical Laboratory,
National Advisory Committee for Aeronautics,
Langley Field, Va., June 18, 1957.

[redacted]

APPENDIX

DERIVATION OF DRAG-COEFFICIENT RELATIONS

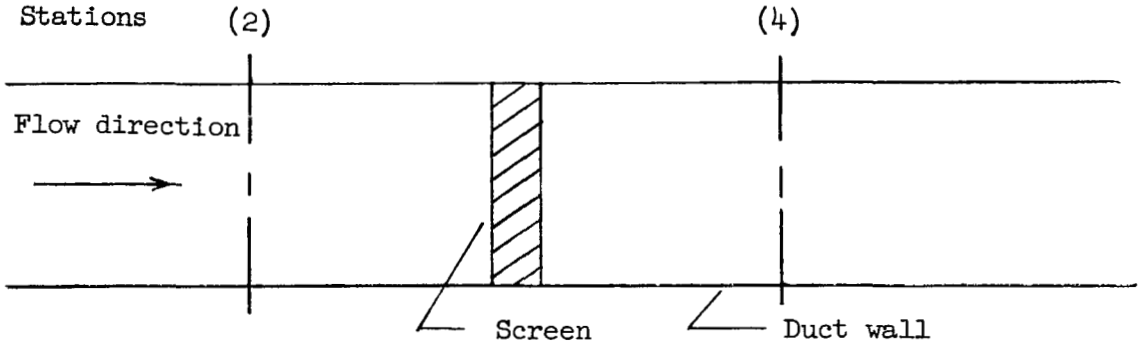

According to the momentum equation the drag of the screen is as follows:

$$D = mu_2 - mu_4 + (p_2 - p_4)A = C_D q_2 (1 - f)A \tag{1}$$

Through substitution of the following relations

$$\left.\begin{aligned} mu &= \gamma p A M^2 \\ q &= \frac{\gamma}{2} p M^2 \end{aligned}\right\} \tag{2}$$

equation (1) may be converted to

$$1 - \frac{p_4}{p_2}\left(1 + \gamma M_4^2\right) = \gamma M_2^2 \left[\frac{C_D}{2}(1 - f) - 1\right] \tag{3}$$

The static pressure ratio may be expressed in terms of Mach number:

$$\frac{p_4}{p_2} = \frac{M_2\sqrt{1 + \frac{\gamma - 1}{2} M_2^2}}{M_4\sqrt{1 + \frac{\gamma - 1}{2} M_4^2}} \tag{4}$$

Substitution of equation (4) into equation (3) produces

$$1 + \gamma M_4^2 = \gamma M_4 \sqrt{1 + \frac{\gamma - 1}{2} M_4^2} \tag{5}$$

where

$$Y \equiv \frac{1 - \gamma M_2^2\left[\frac{C_D}{2}(1 - f) - 1\right]}{M_2\sqrt{1 + \frac{\gamma - 1}{2} M_2^2}} \tag{6}$$

Solving equation (5) for M_4 gives

$$M_4^2 = \frac{\left(1 - \frac{2\gamma}{Y^2}\right) \pm \sqrt{1 - \frac{2(\gamma + 1)}{Y^2}}}{\left[\frac{2\gamma^2}{Y^2} - (\gamma - 1)\right]} \tag{7}$$

Thus, the downstream Mach number M_4 can be determined directly from Y, which according to equation (6) is a function of upstream Mach number M_2 and the drag coefficient $C_D(1 - f)$. The total pressure ratio can be evaluated by using the following expression:

$$\frac{H_4}{H_2} = \frac{p_4}{p_2}\left(\frac{1 + \frac{\gamma - 1}{2} M_4^2}{1 + \frac{\gamma - 1}{2} M_2^2}\right)^{\frac{\gamma}{\gamma - 1}} \tag{8}$$

where the static pressure ratio is given in equation (4). Through use of equations (6), (7), (4), and (8) in that order the drag-coefficient curves of figure 19 were calculated.

REFERENCES

1. Adler, Alfred A.: Variation With Mach Number of Static and Total Pressures Through Various Screens. NACA WR L-23, 1946. (Formerly NACA CB L5F28.)

2. Eckert, B., and Pflüger, F.: The Resistance Coefficient of Commercial Round Wire Grids. NACA TM 1003, 1942.

3. Hoerner, S. F.: Pressure Losses Across Screens and Grids. AF Tech. Rep. No. 6289, Wright Air Dev. Center, U. S. Air Force, Nov. 1950.

4. Collar, A. R.: The Effect of a Gauze on the Velocity Distribution in a Uniform Duct. R. & M. No. 1867, British A.R.C., 1939.

5. Baines, W. D., and Peterson, E. G.: An Investigation of Flow Through Screens. Trans. A.S.M.E., vol. 73, no. 5, July 1951, pp. 467-480.

6. Schubauer, G. B., and Spangenberg, W. G.: Effect of Screens in Wide-Angle Diffusers. NACA Rep. 949, 1949.

7. Schubauer, G. B., Spangenberg, W. G., and Klebanoff, P. S.: Aerodynamic Characteristics of Damping Screens. NACA TN 2001, 1950.

[redacted]

TABLE I.- SCREEN VARIABLES

Screen solidity ratio, 1 - f	Rod diameter, in.	b, in.	c, in.	Angle of sweep, ψ, deg
Screen shape I				
0.165	$\frac{1}{8}$	0.308	0.783	0
.234	$\frac{1}{8}$	.145	.481	0 15 30 45 75
.265	$\frac{1}{8}$	.110	.401	45
.302	$\frac{1}{8}$	.080	.329	0 30 45 60
.371	$\frac{1}{8}$	.040	.238	60
.427	$\frac{1}{8}$	.000	.178	75
.265	$\frac{1}{16}$	.010	.201	45
.265	$\frac{1}{4}$	.316	.801	45
.371	$\frac{1}{4}$	.138	.107	60
.265	Streamline rods	.056	.287	45
Screen shape II				
0.302	$\frac{1}{8}$	0.080	0.329	45
Screen shape III				
0.302	$\frac{1}{8}$	0.080	0.329	M, W

[redacted]

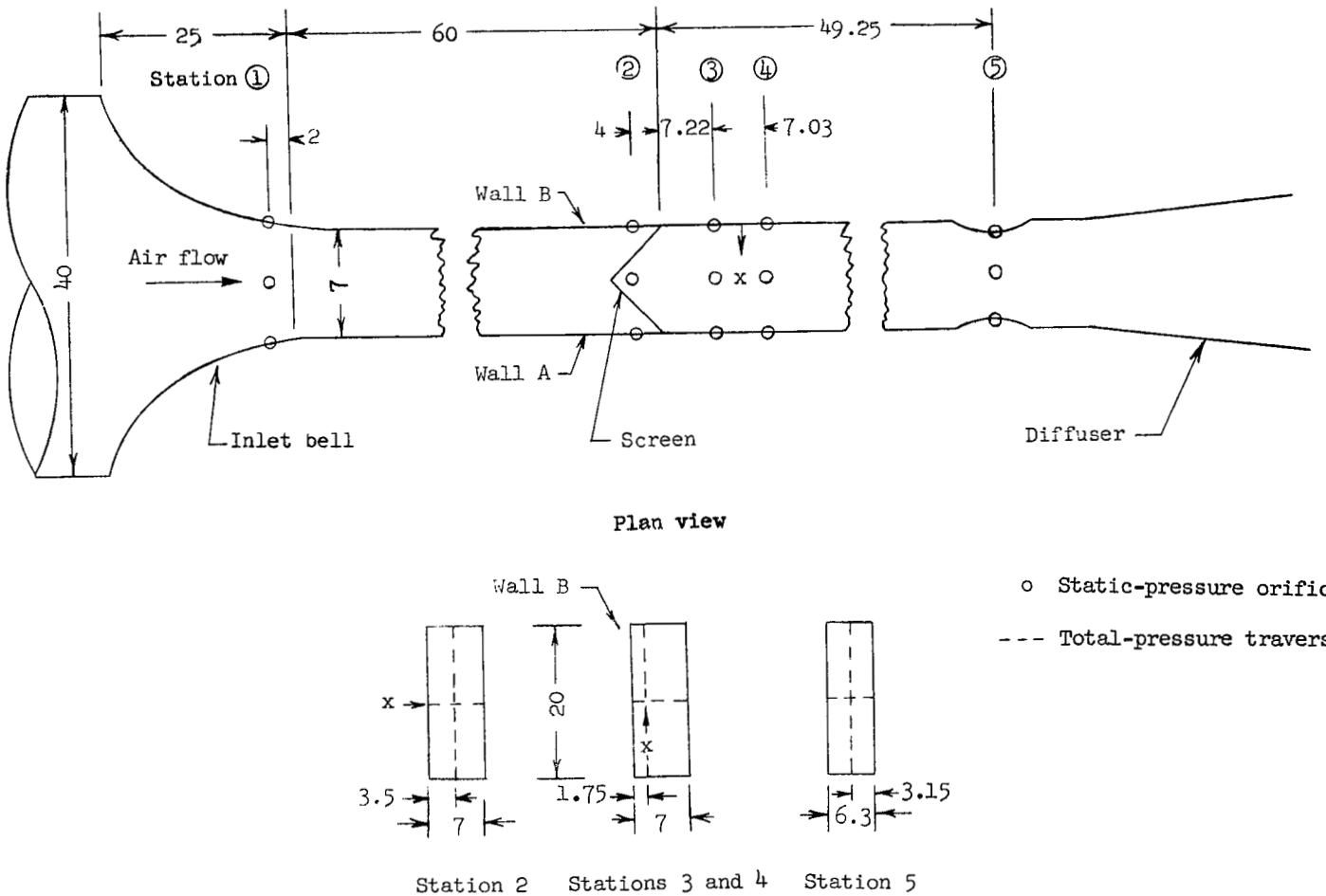

Figure 1.- Diagram of rectangular-channel test setup. All dimensions are in inches.

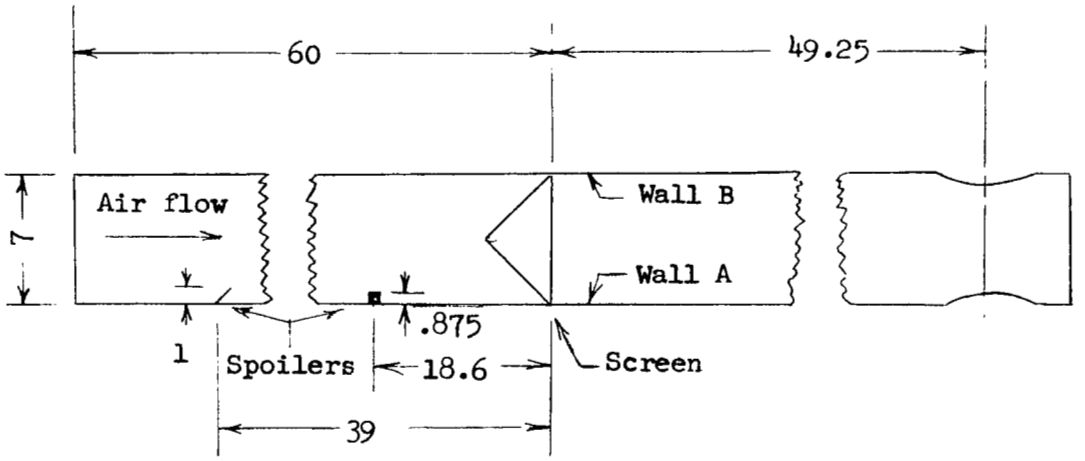

(a) Configuration I.

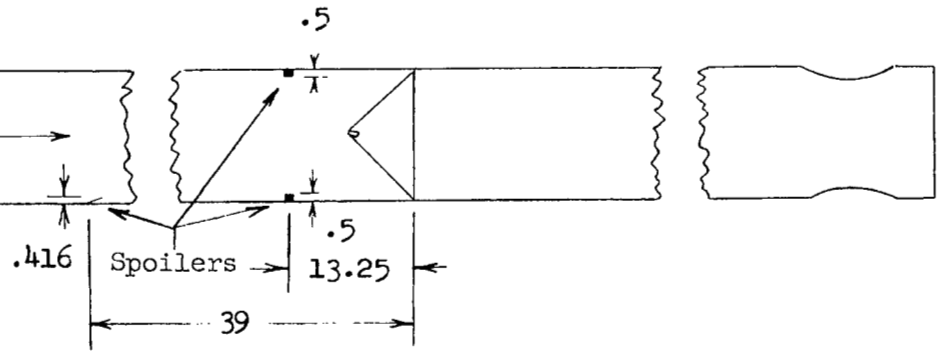

(b) Configuration II.

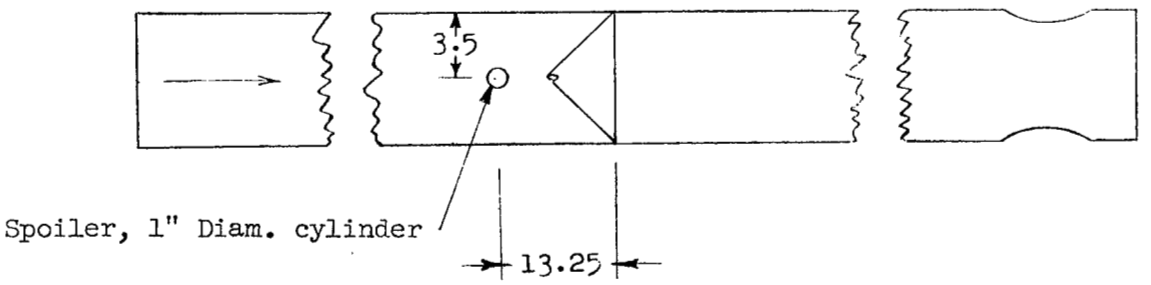

(c) Configuration III.

Plan view

Figure 2.- Details of test configurations I, II, and III. All dimensions are in inches.

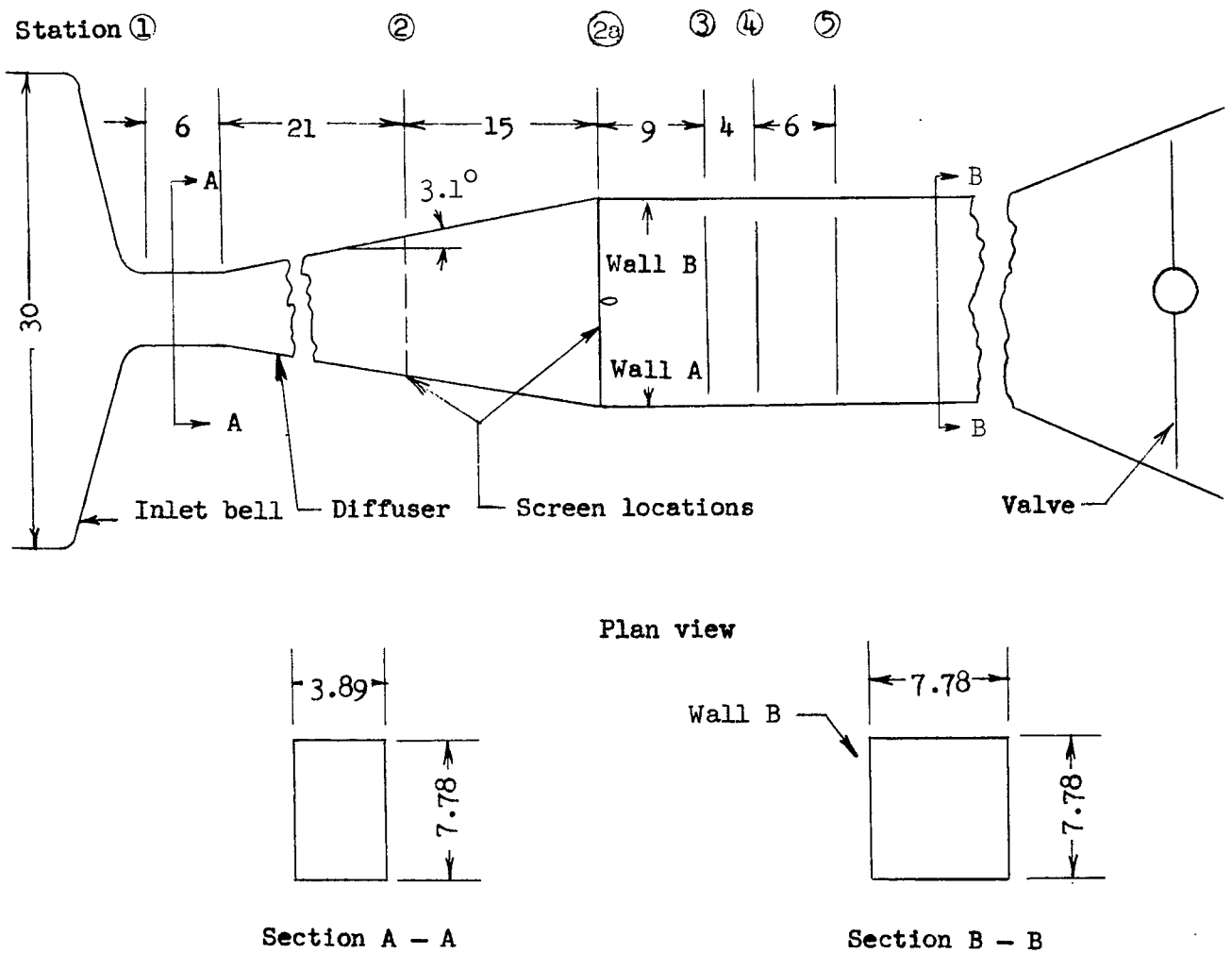

Figure 3.- Diagram of diffuser test setup. All dimensions are in inches.

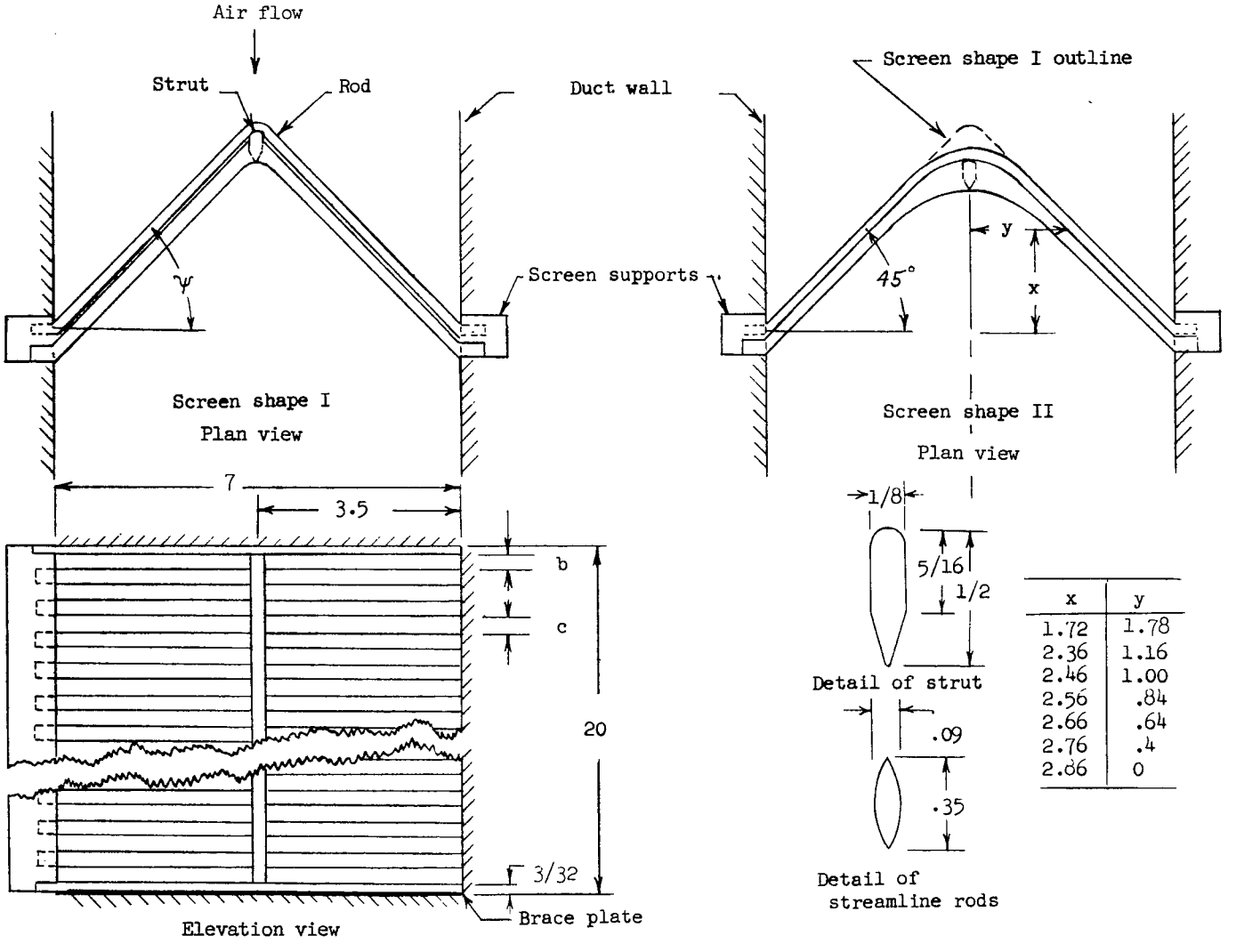

x	y
1.72	1.78
2.36	1.16
2.46	1.00
2.56	.84
2.66	.64
2.76	.4
2.86	0

Figure 4.- Drawings showing screen shapes I and II and detail of strut and streamline rod. All dimensions are in inches.

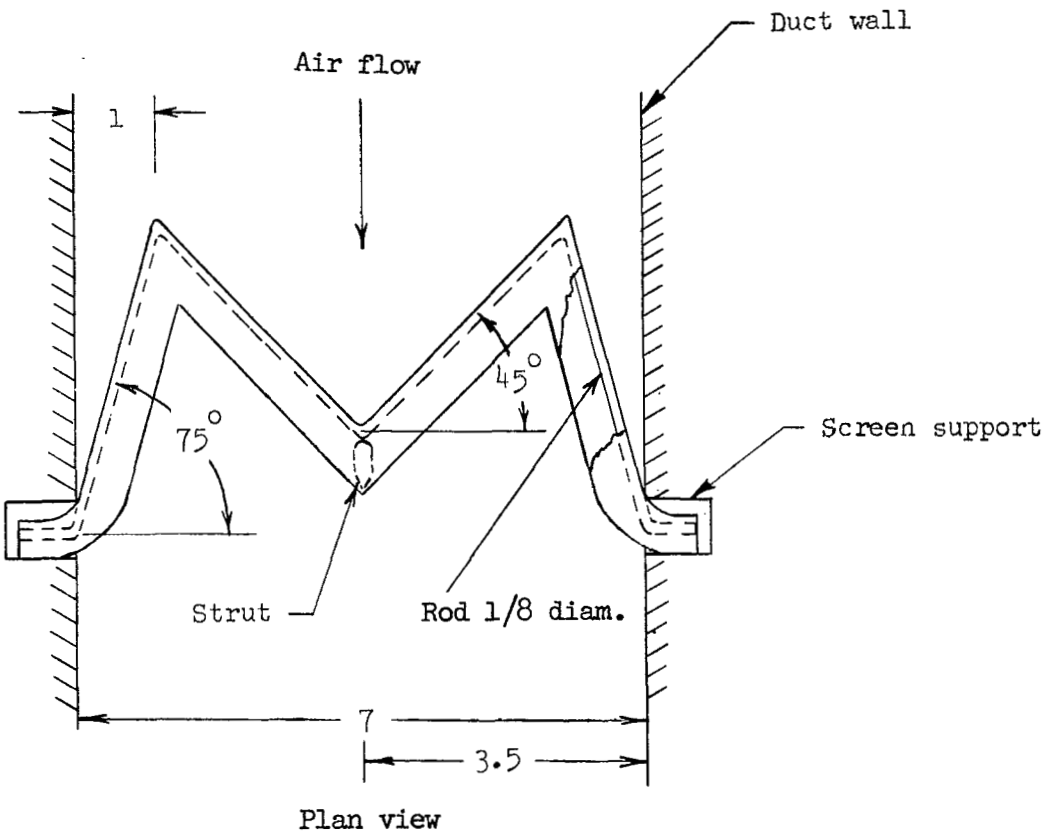

M position shown; reverse for W position

Figure 5.- Drawing showing screen shape III. All dimensions are in inches unless otherwise indicated.

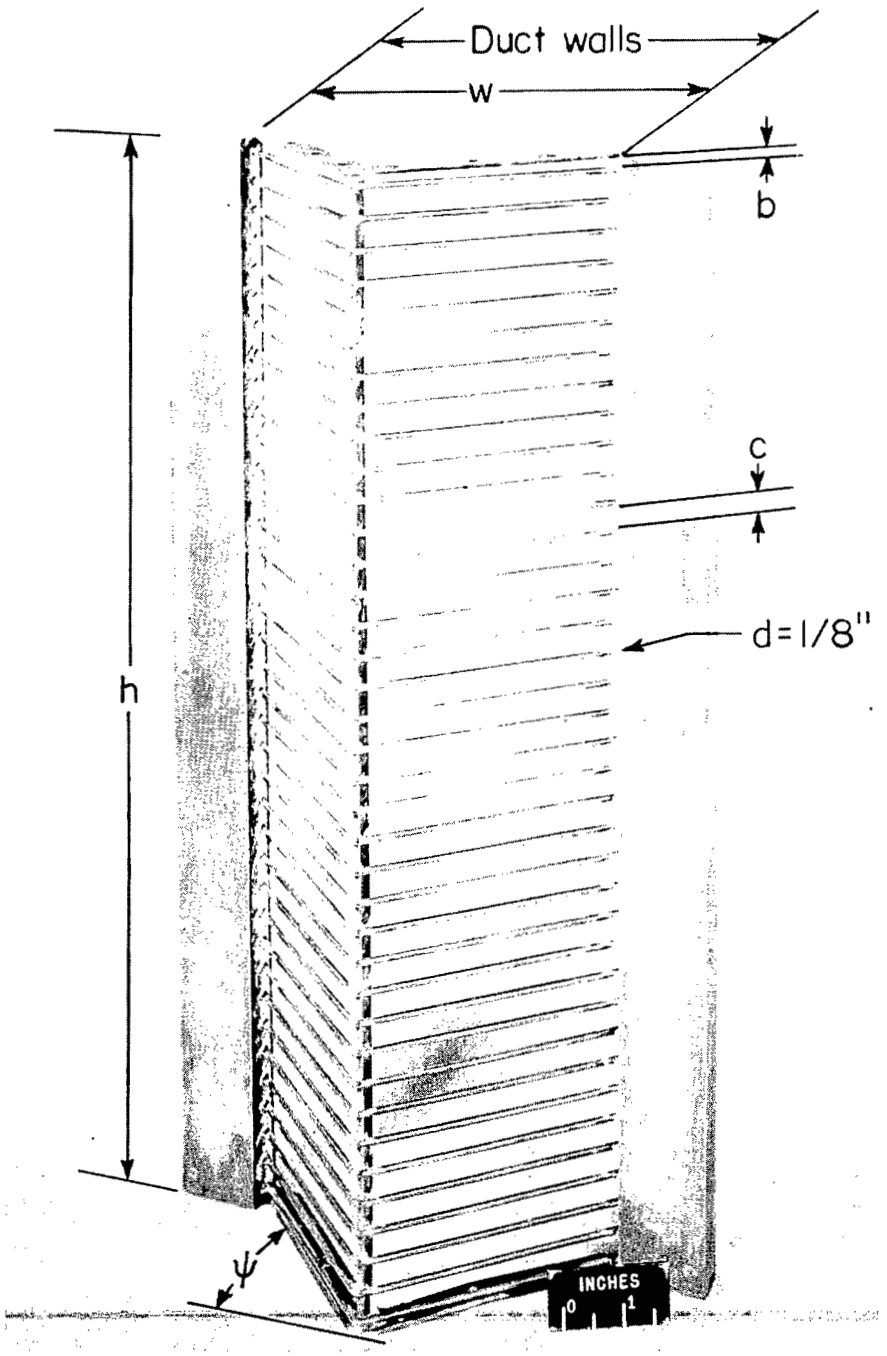

Figure 6.- Screen shape I. L-94052.1

[redacted]

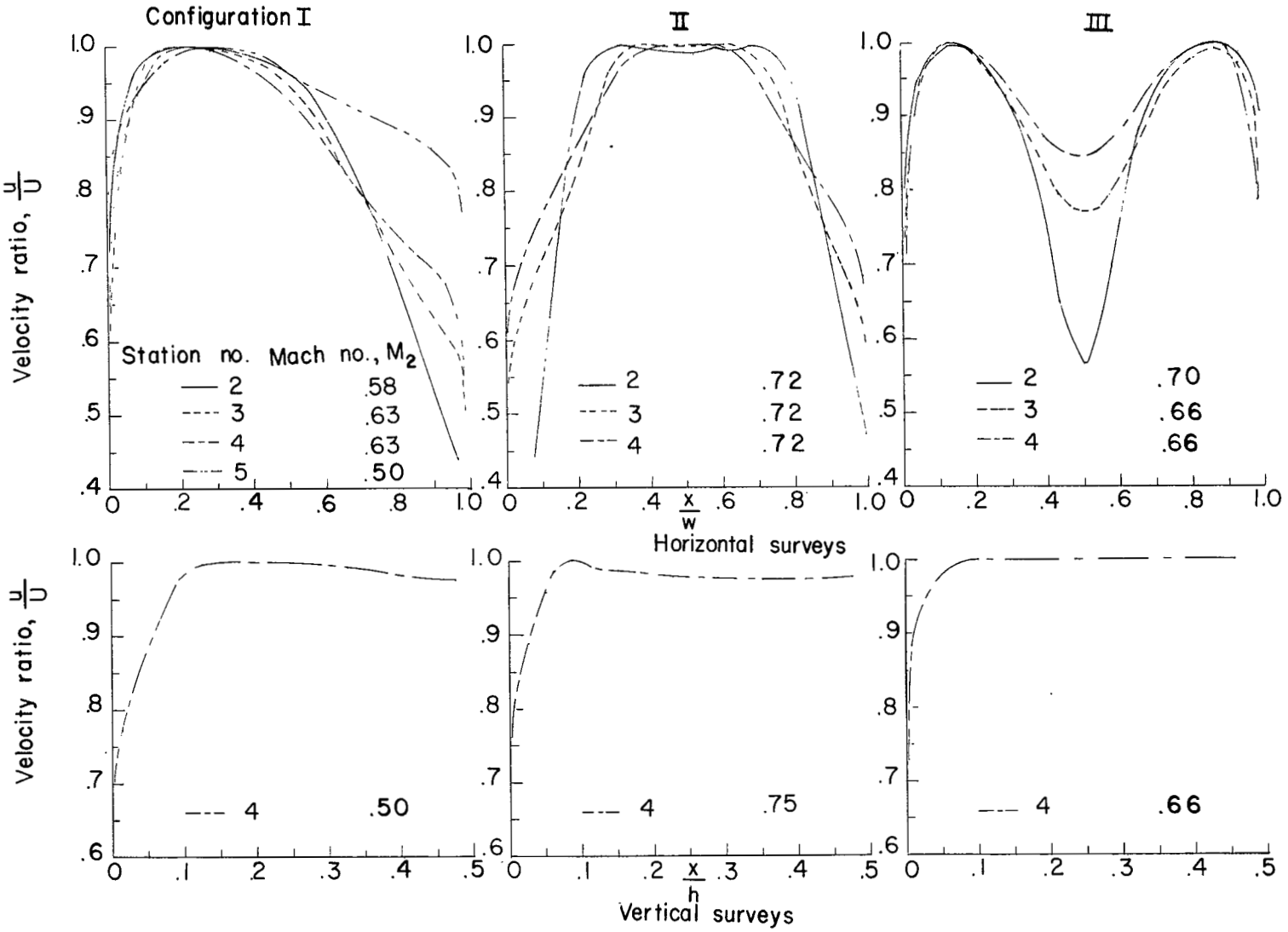

Figure 7.- Velocity distributions at several stations with no screen. Configurations I, II, and III.

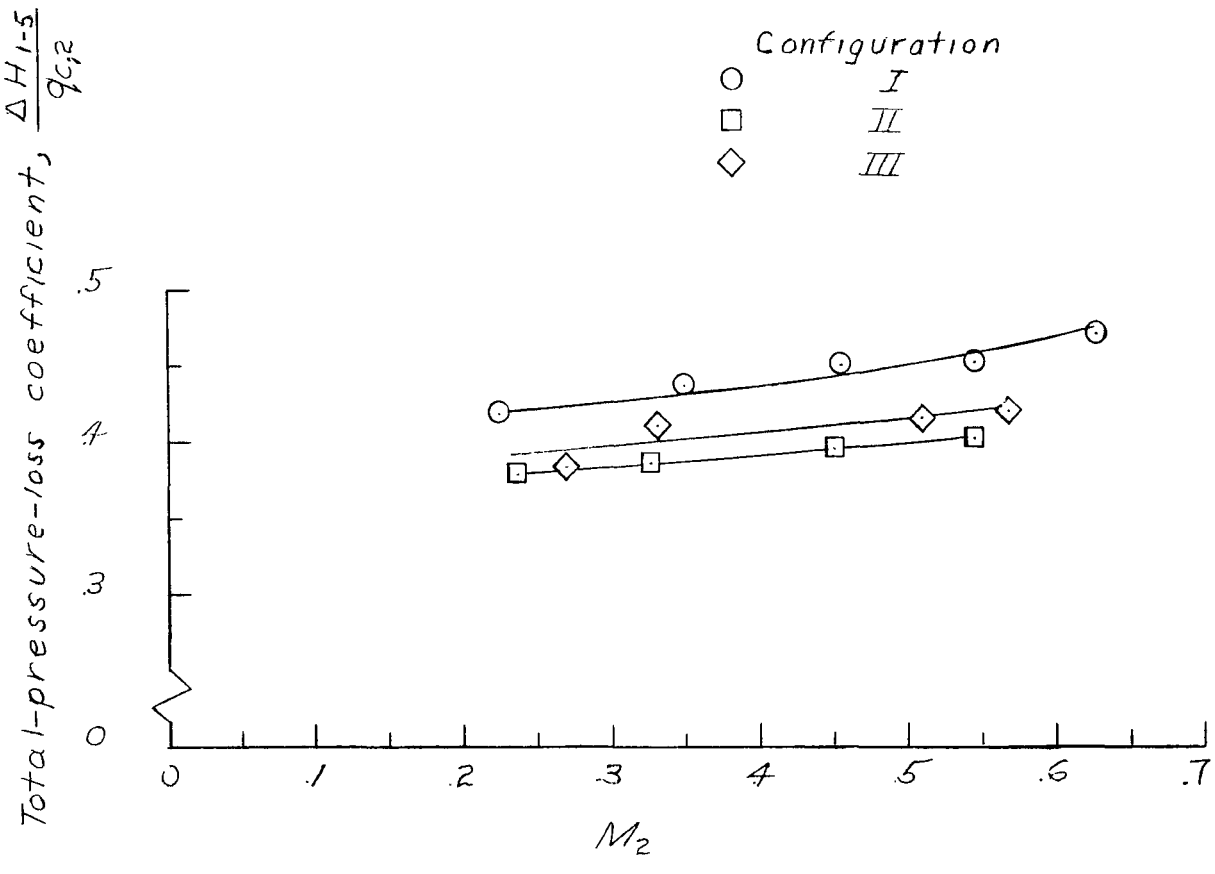

Figure 8.- Duct loss coefficient with no screens. Configurations I, II, and III.

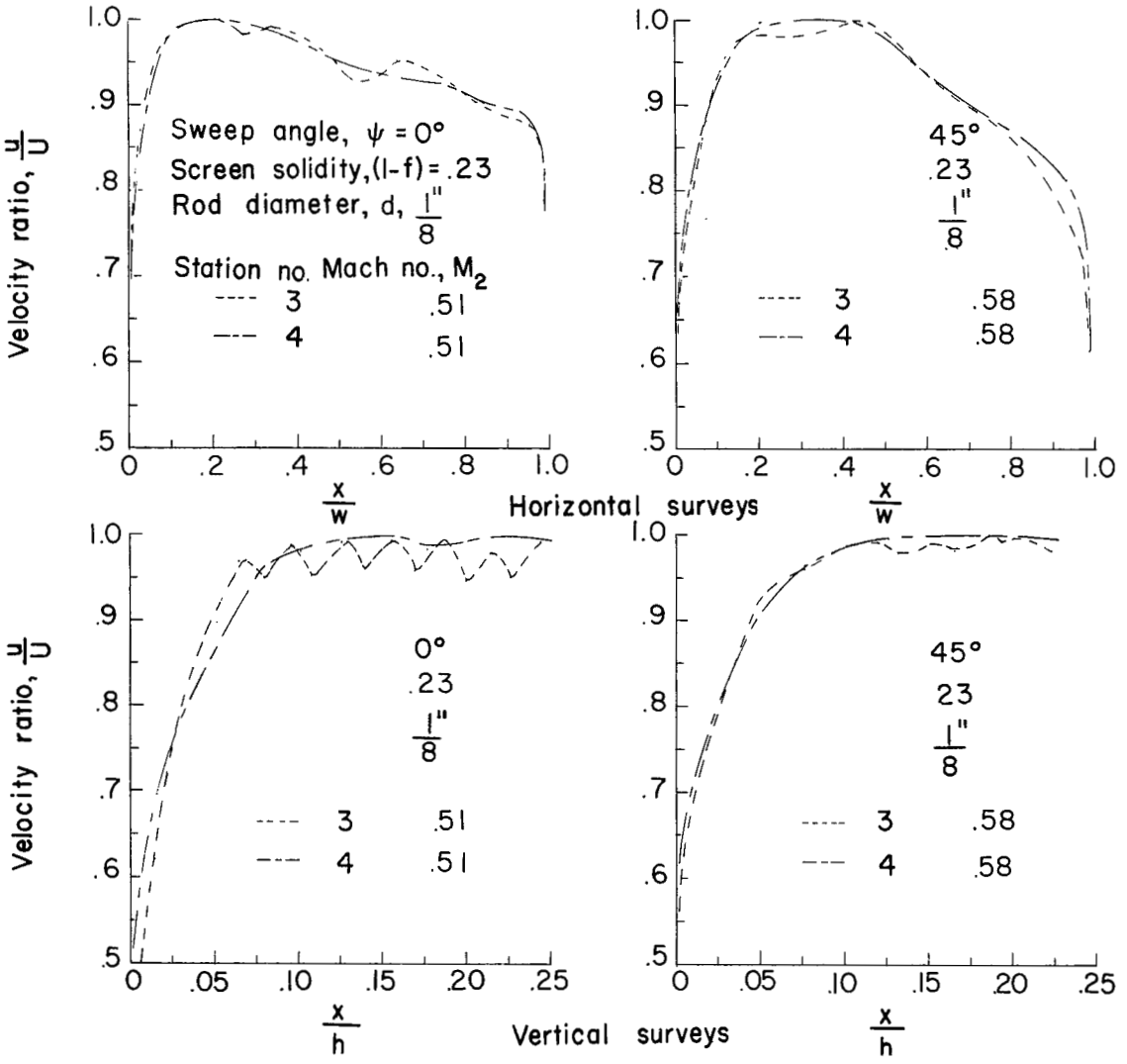

Figure 9.- Typical vertical and horizontal velocity distributions downstream from screens. Configuration I.

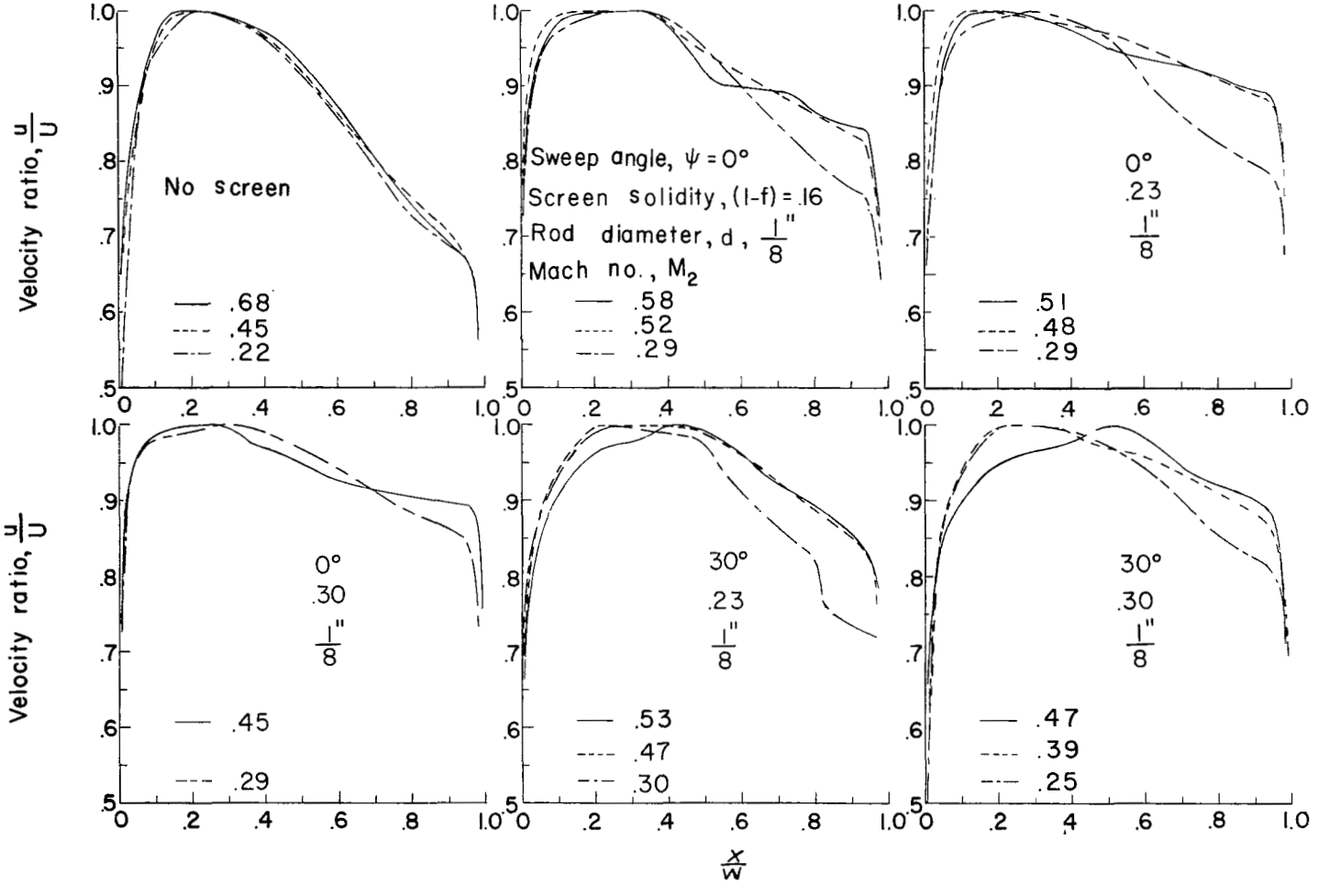

(a) No screen and screens at sweep angles of 0° and 30°.

Figure 10.- Velocity distributions at station 4. Configuration I. (Unless otherwise noted, swept screens of shape I design.)

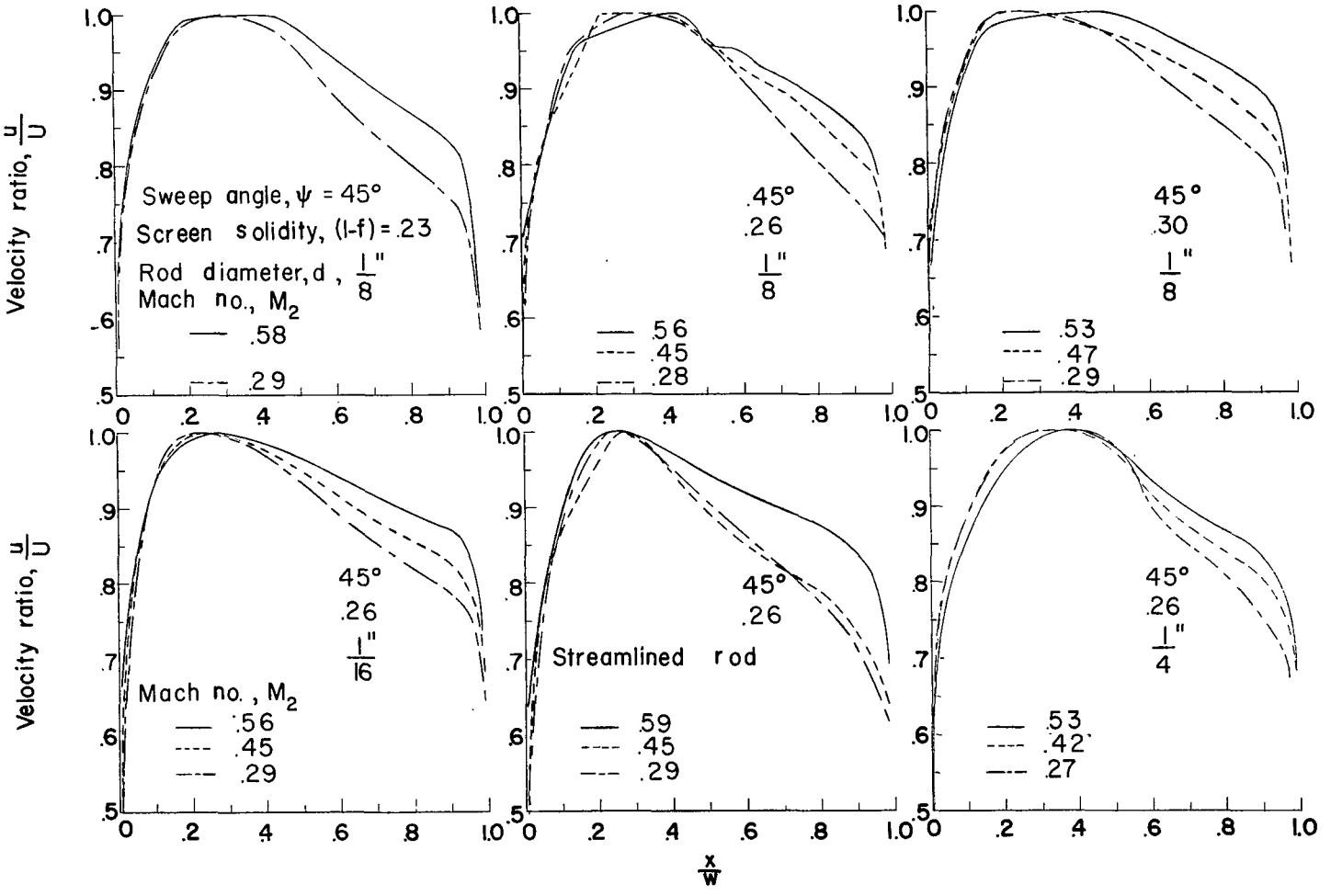

(b) Sweep angle of 45°.

Figure 10.- Continued.

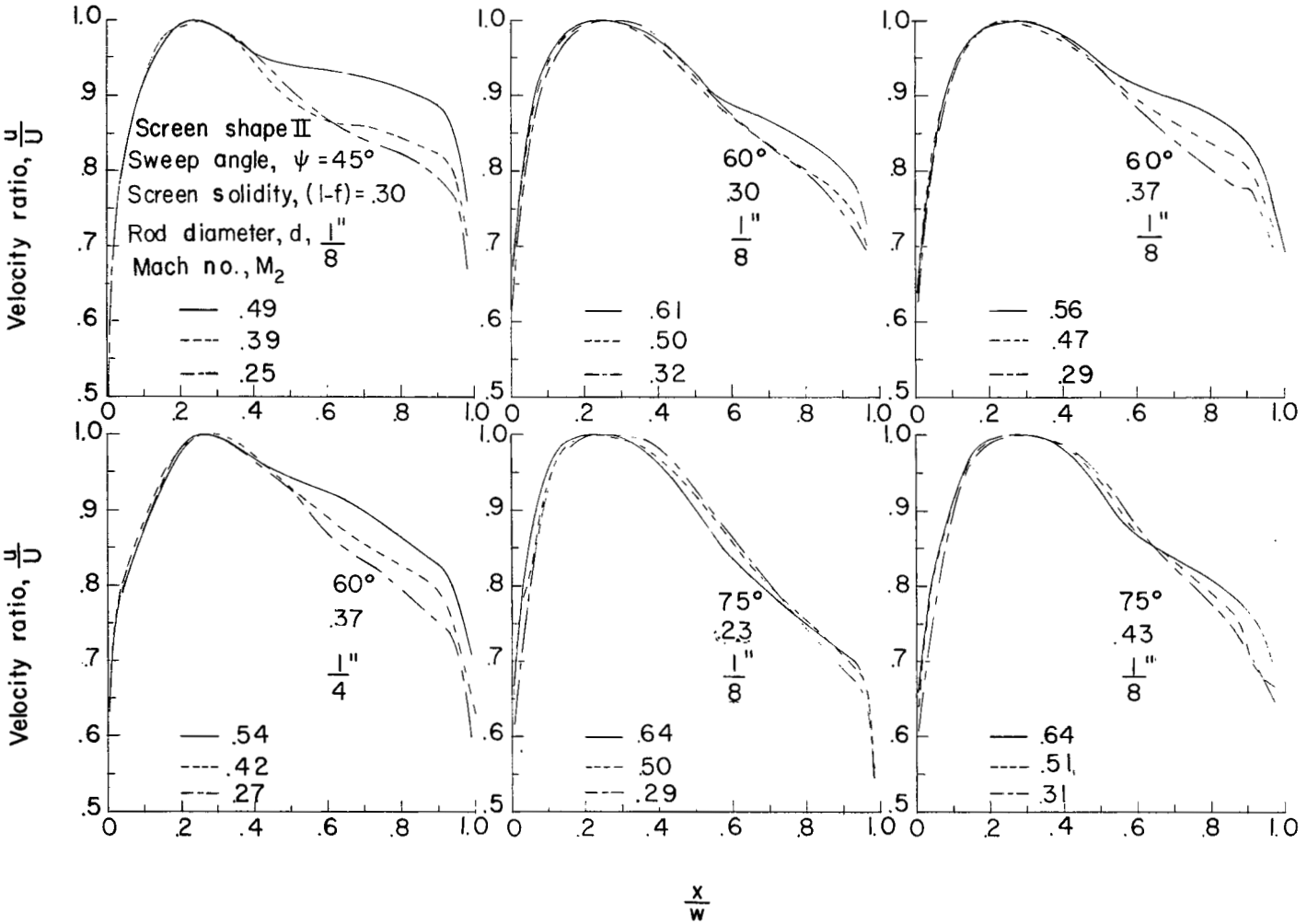

(c) Screen shape II and sweep angles of 60° and 75°.

Figure 10.- Continued.

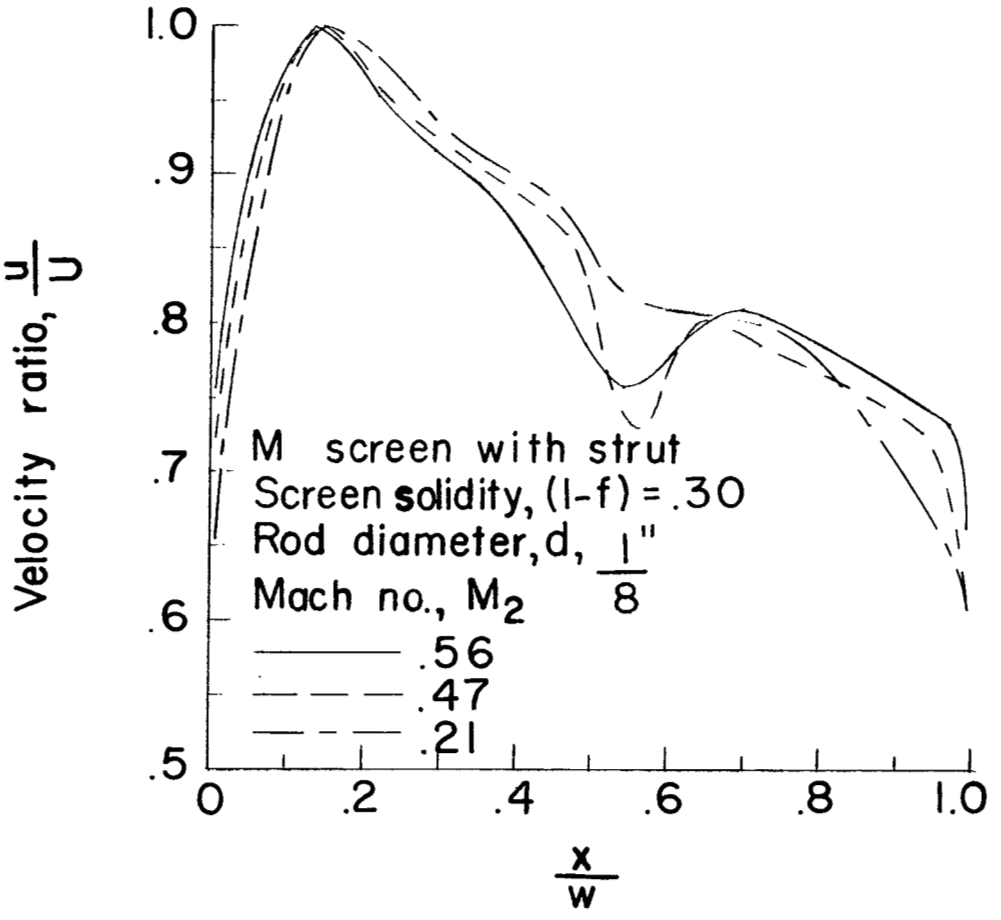

(d) M-screen with strut.

Figure 10.- Concluded.

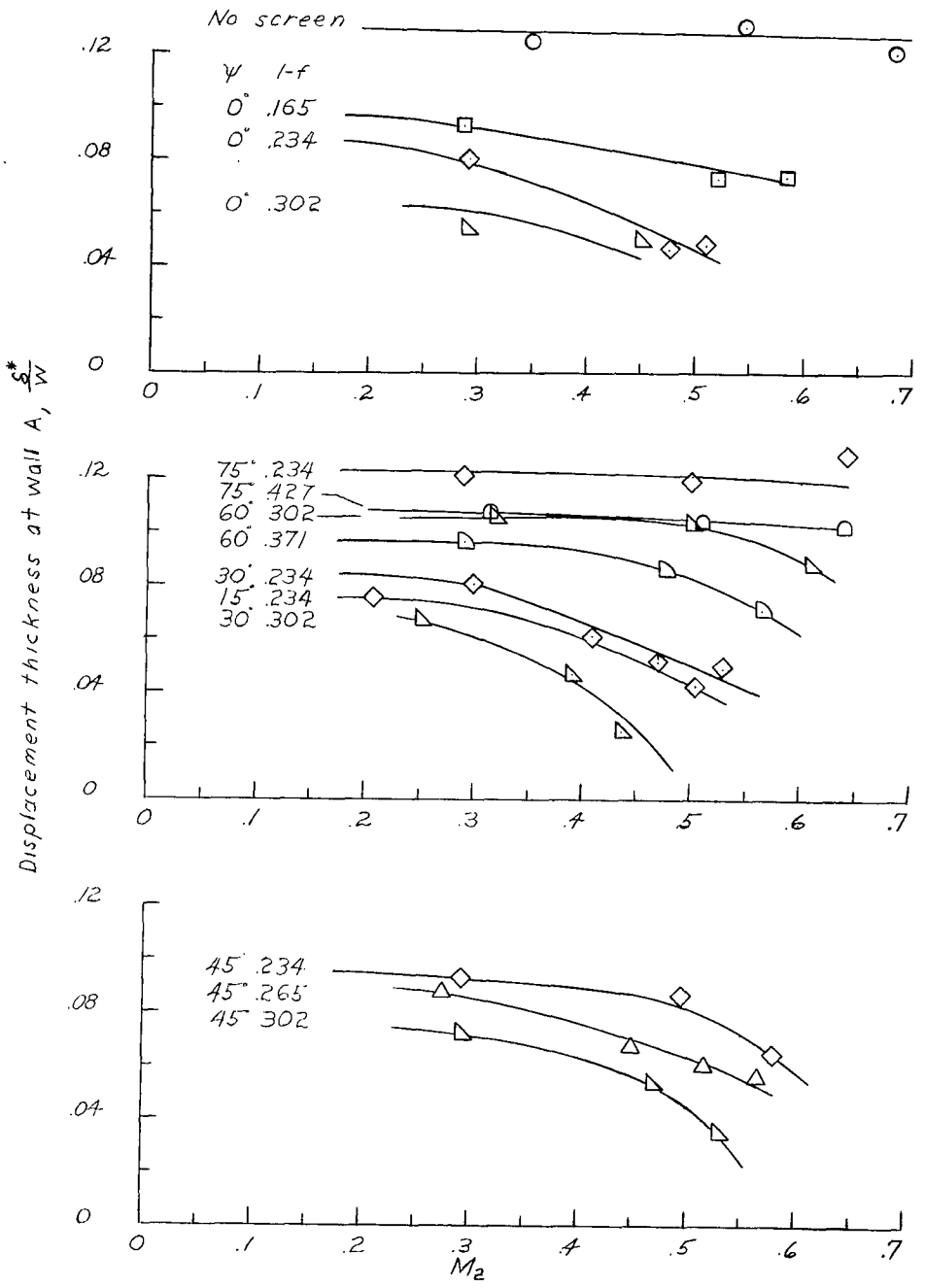

(a) Shape I screens.

Figure 11.- Displacement thickness of wall A as a function of screen inlet Mach number. Configuration I.

[redacted]

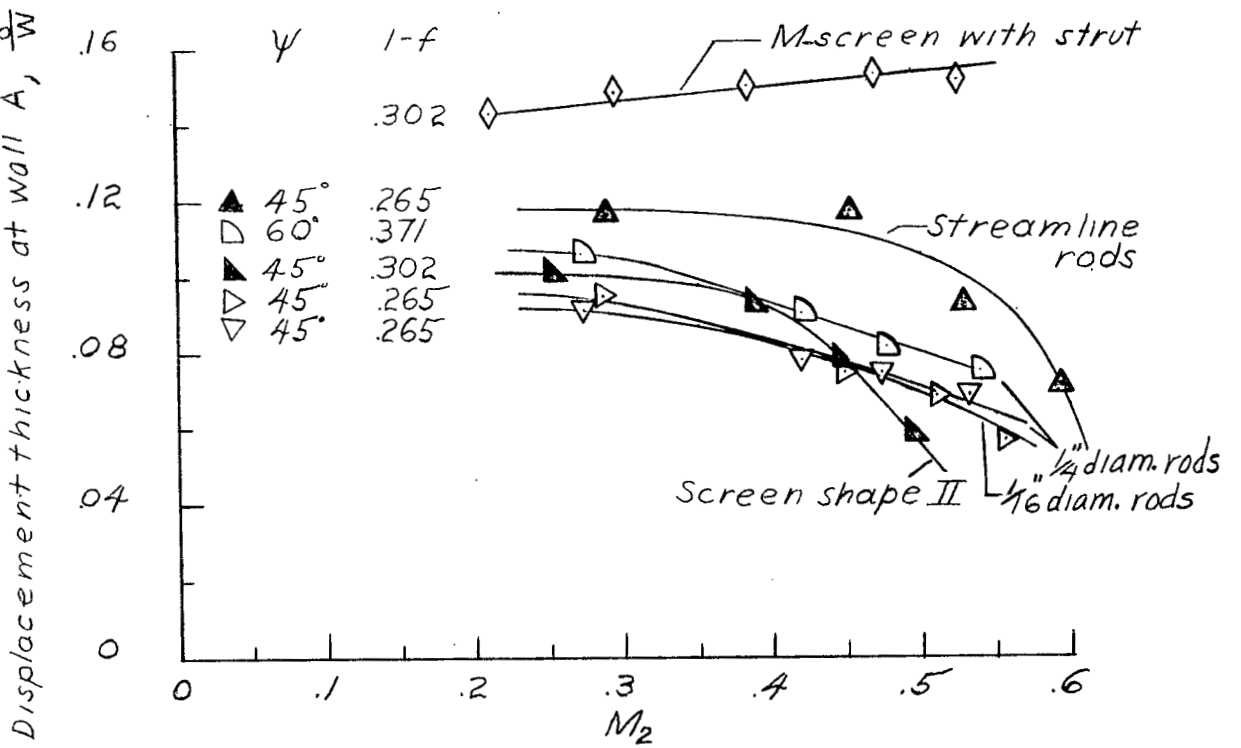

(b) Special screens.

Figure 11.- Concluded.

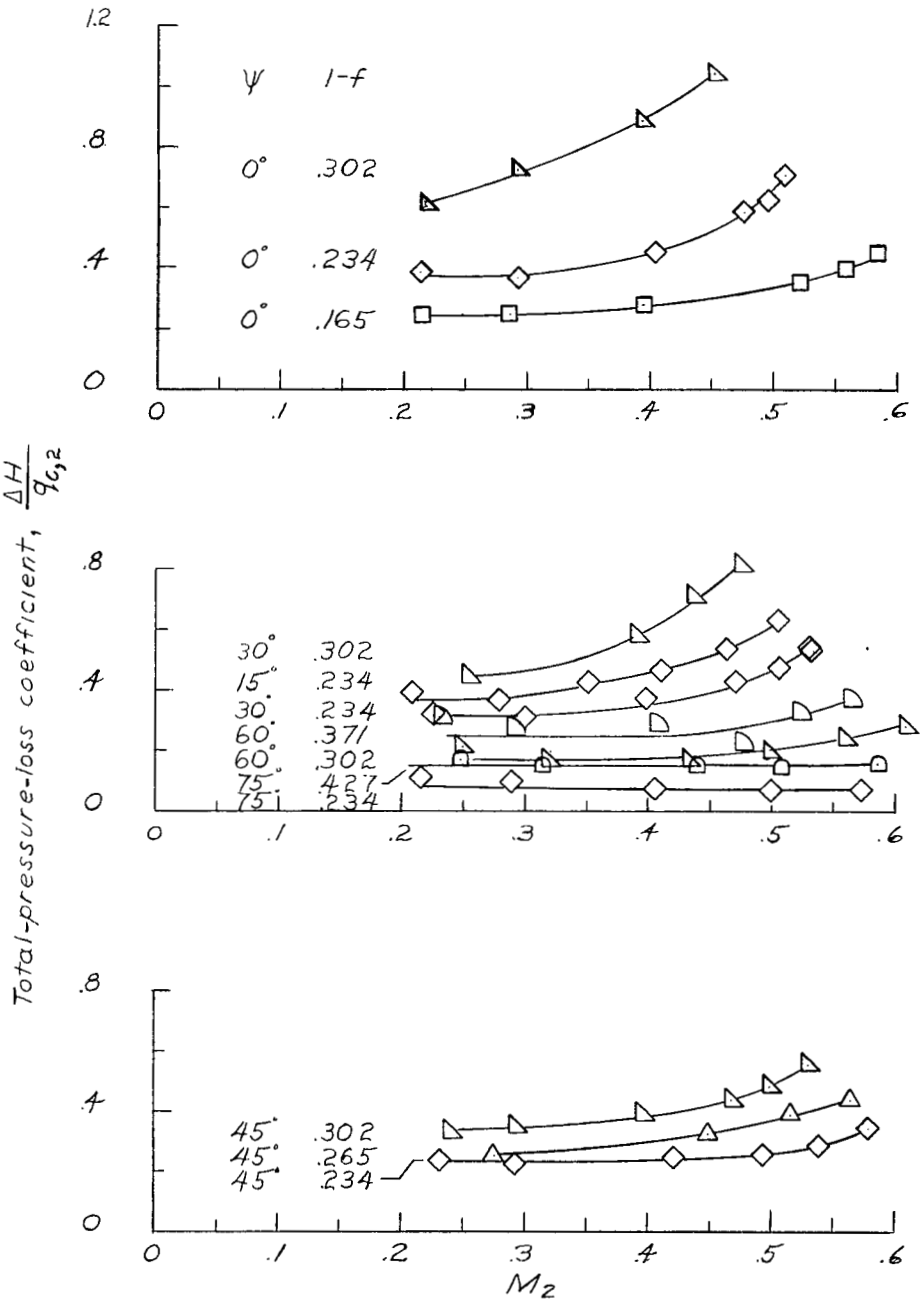

(a) Shape I screens with 1/8-inch rods.

Figure 12.- Total-pressure-loss coefficient as a function of screen inlet Mach number for the screens tested. Configuration I.

(b) Special screens.

Figure 12.- Concluded.

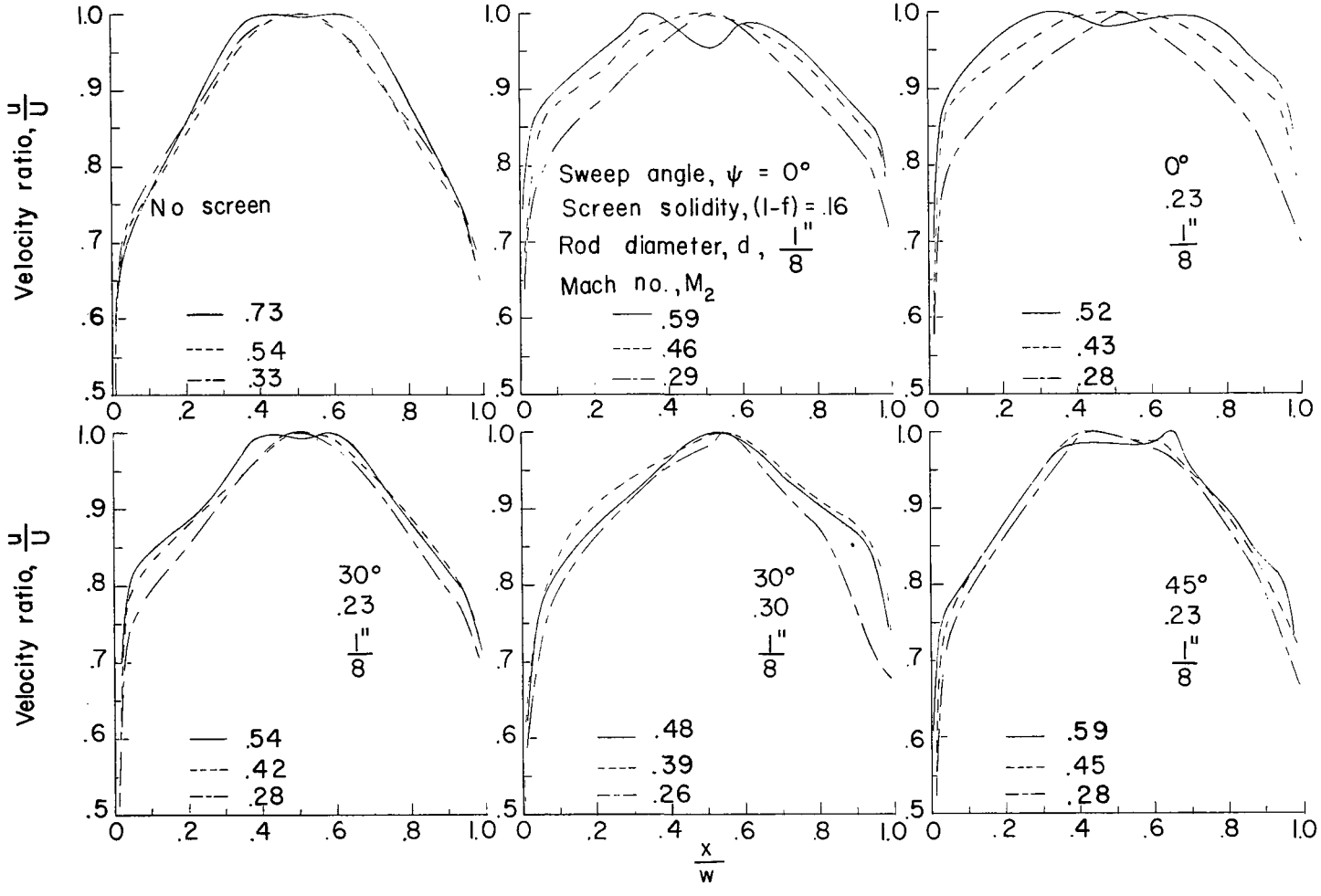

(a) No screen and screens at sweep angles of 0°, 30°, and 45°.

Figure 13.- Velocity distributions at station 4. Configuration II. (Unless otherwise noted, swept screens are of shape I design.)

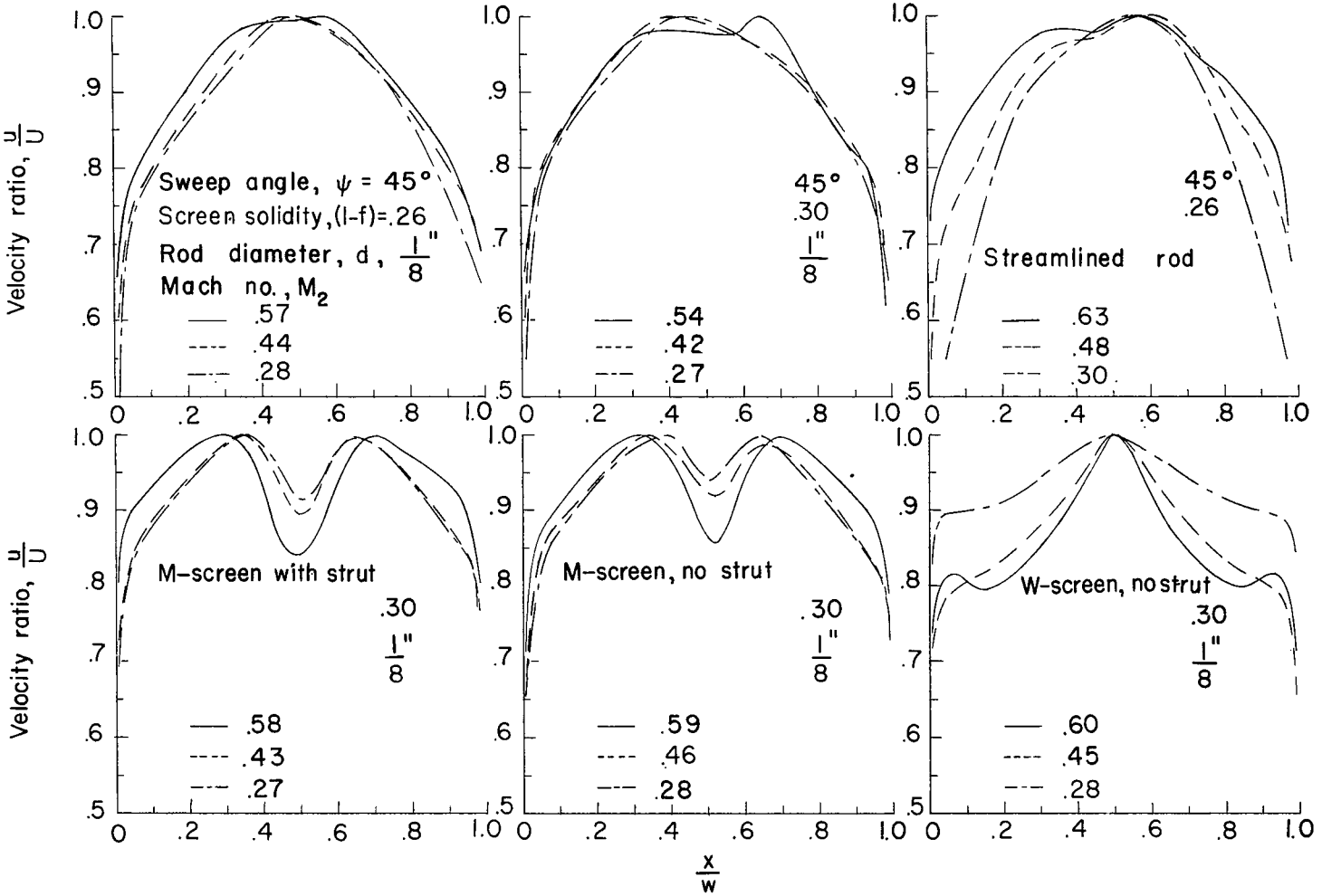

(b) Screen shape I for sweep angle of 45° and special screens.

Figure 13.- Concluded.

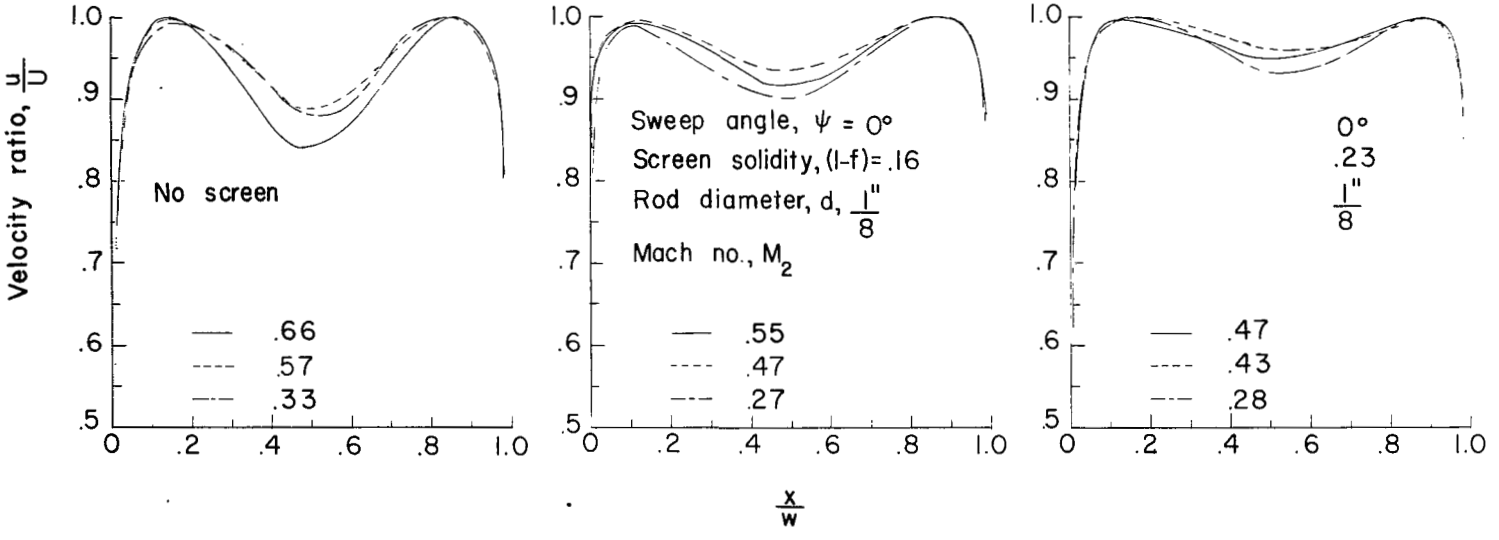

(a) No screen and screens of 0° sweep angle.

Figure 14.- Velocity distributions at station 4. Configuration III.

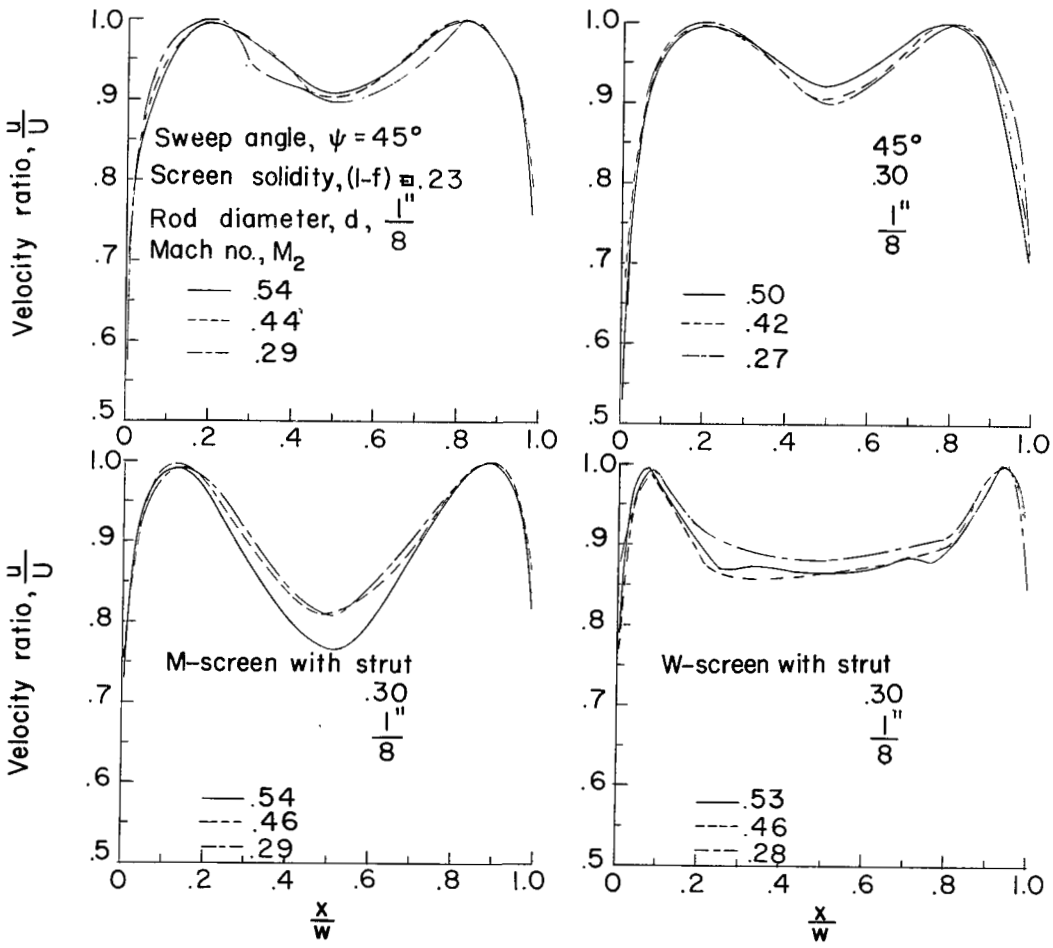

(b) Swept screens of shape I design and special screens.

Figure 14.- Concluded.

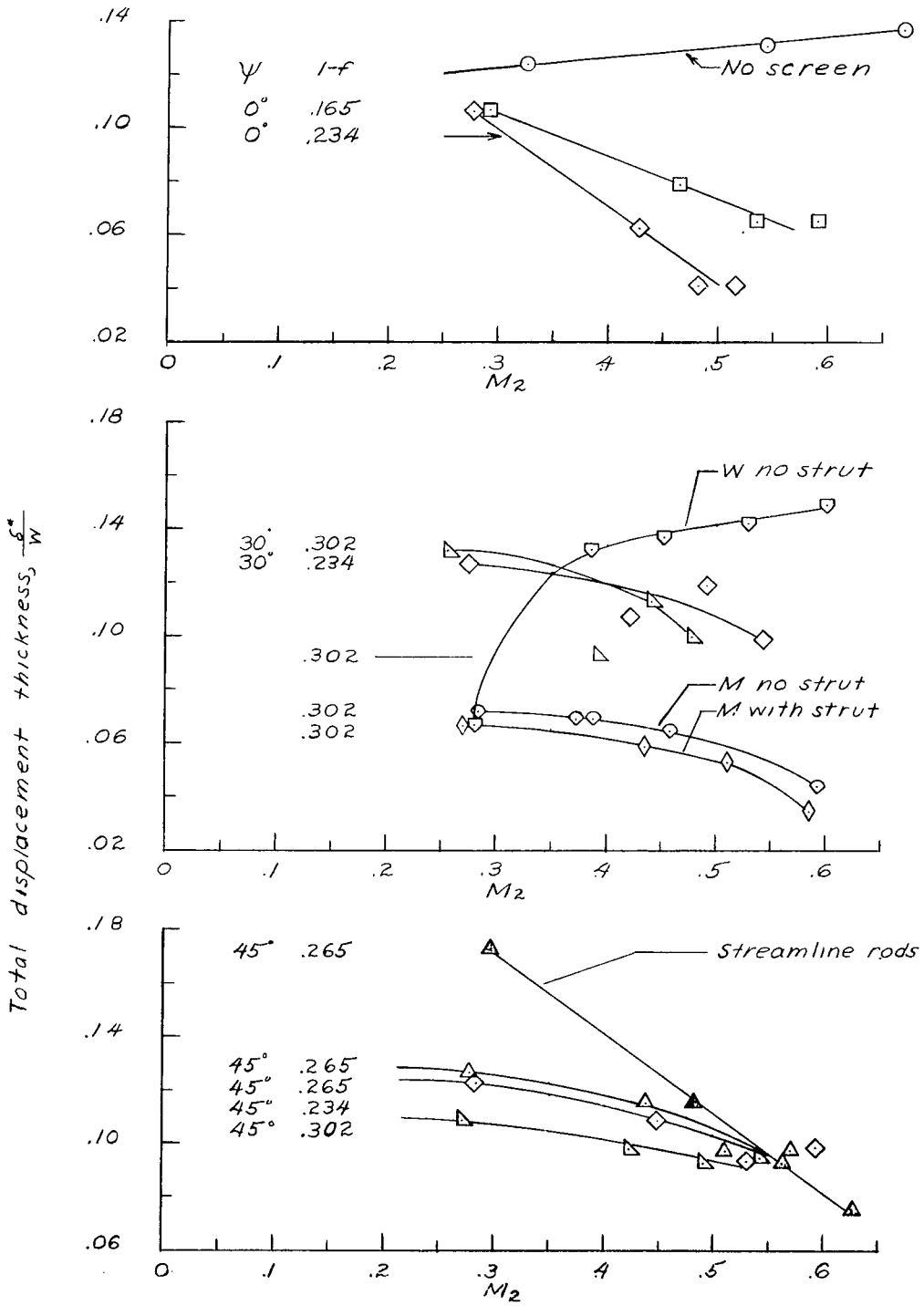

Figure 15.- Total displacement thickness of walls A and B as a function of screen inlet Mach number for the screens tested. Configuration II.

[redacted]

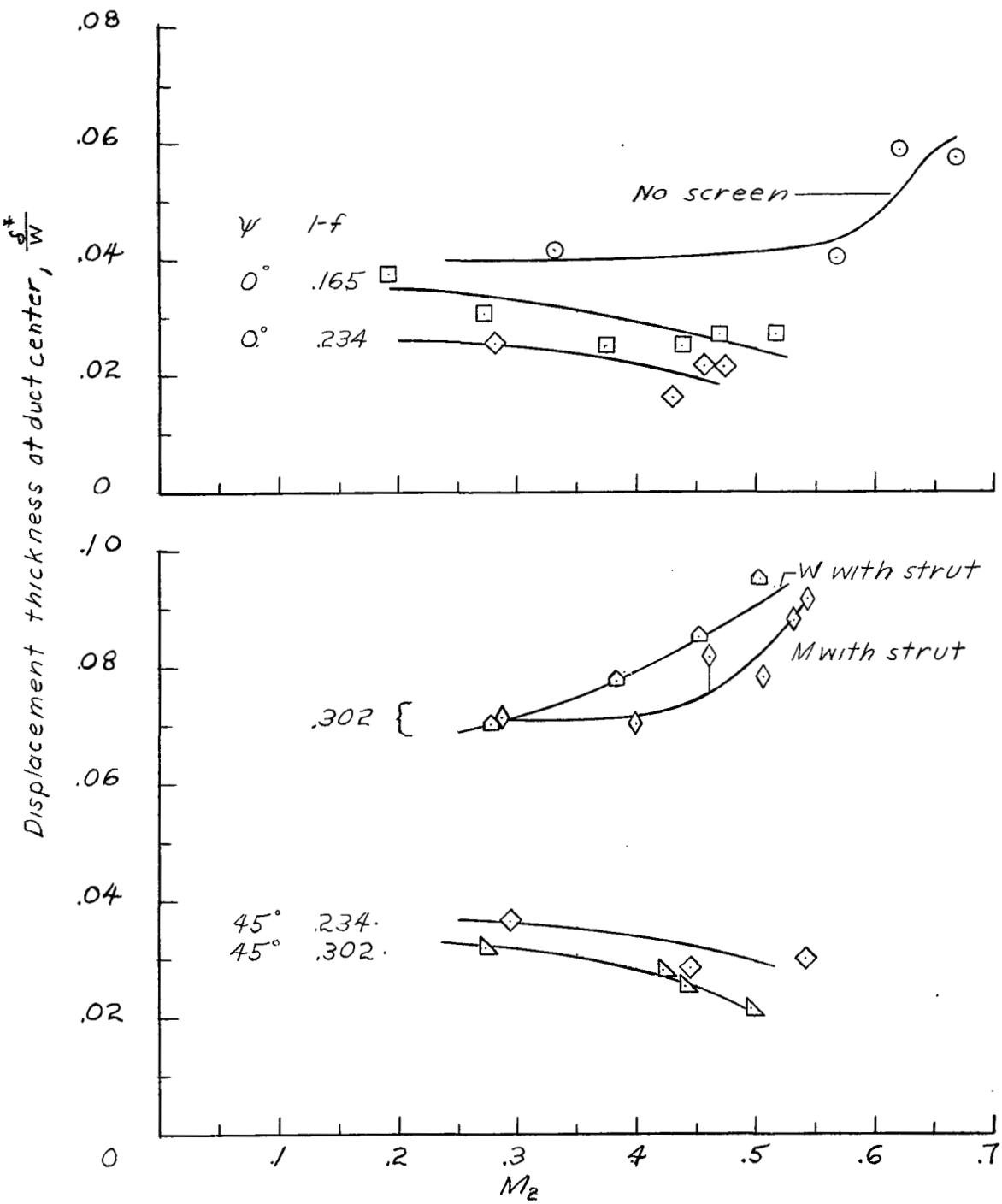

Figure 16.- Displacement thickness as a function of screen inlet Mach number for the screens tested. Configuration III.

[redacted]

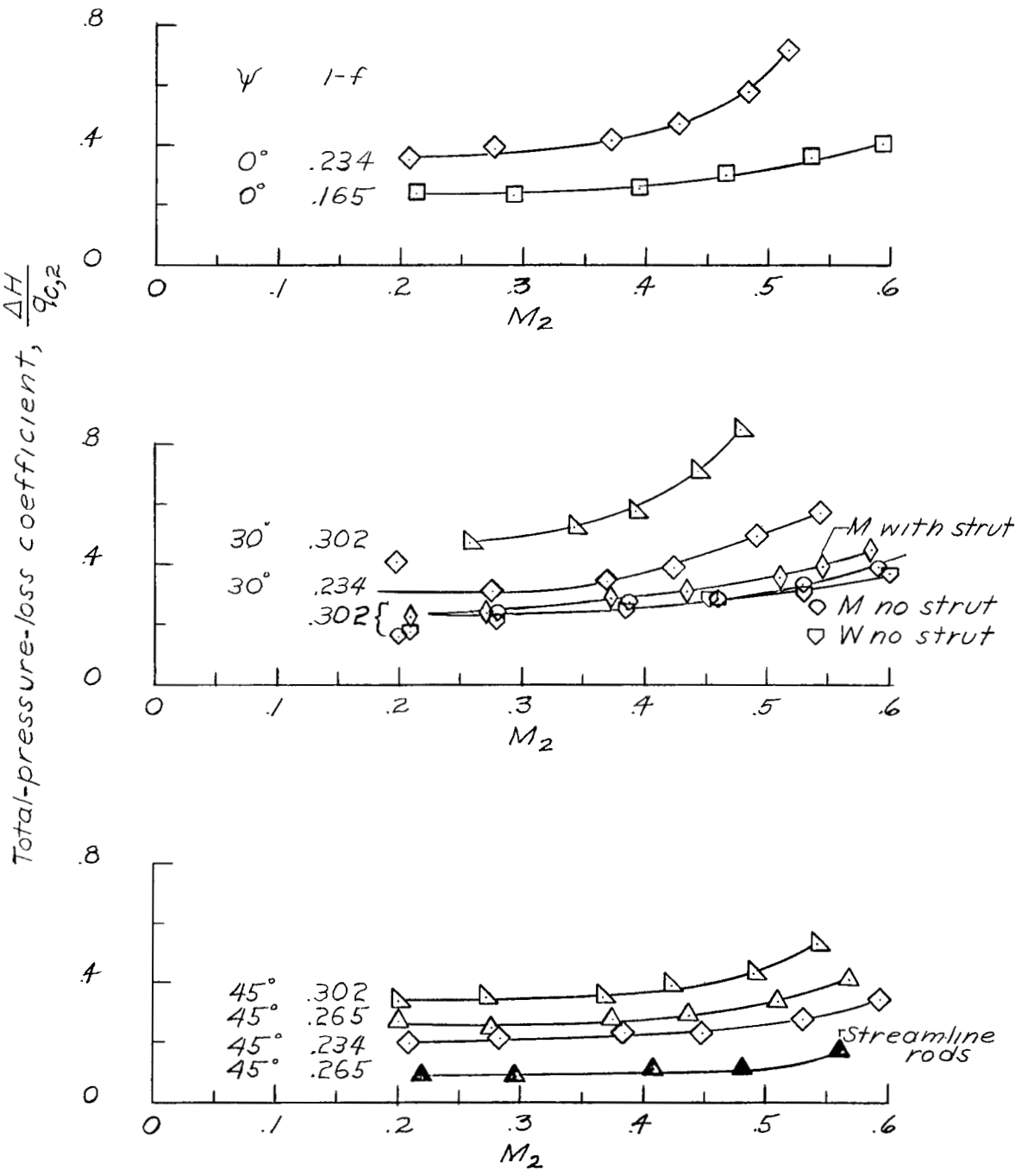

Figure 17.- Total-pressure-loss coefficient as a function of screen inlet Mach number for the screens tested. Configuration II.

[redacted]

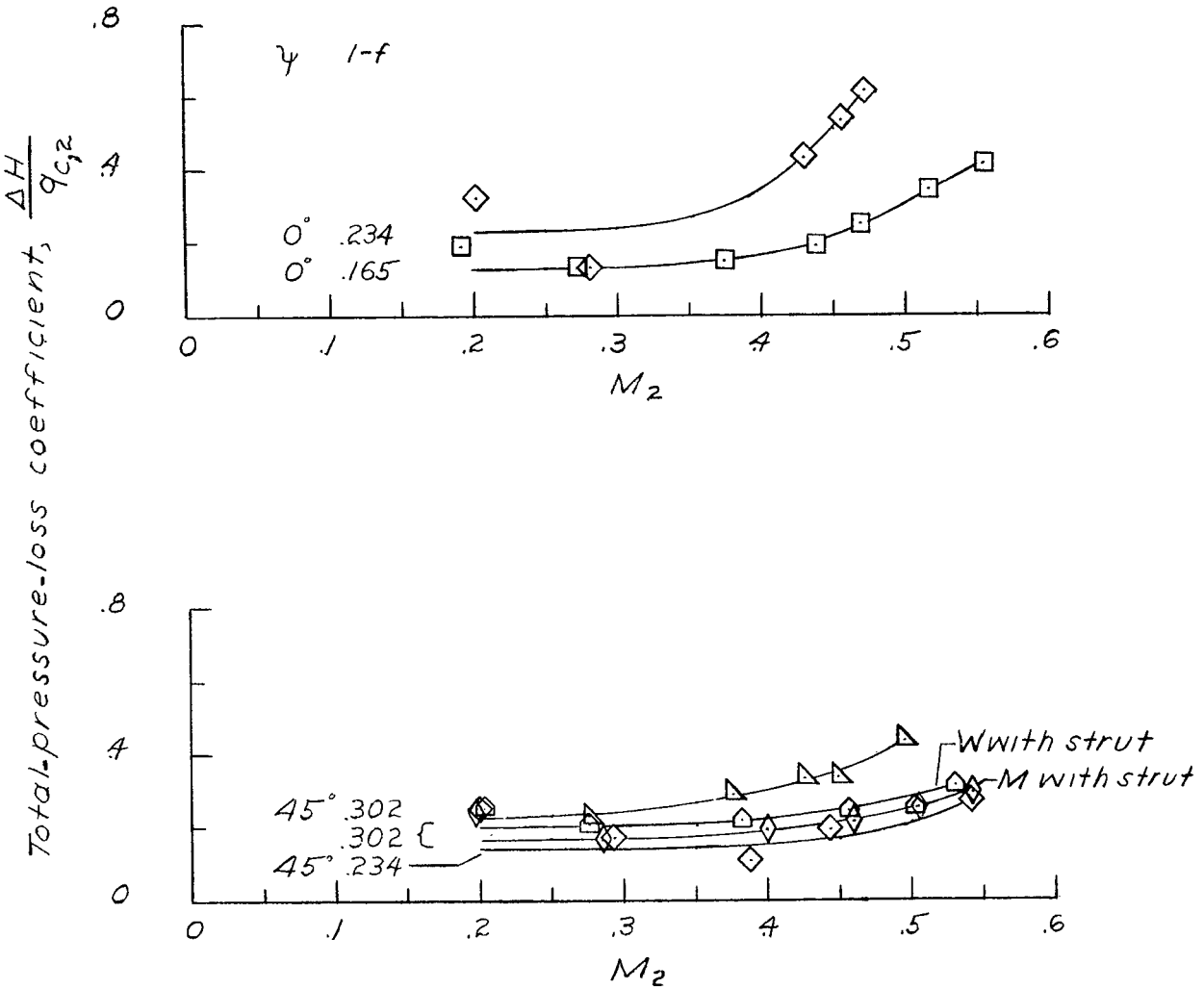

Figure 18.- Total-pressure-loss coefficient as a function of screen inlet Mach number for the screens tested. Configuration III.

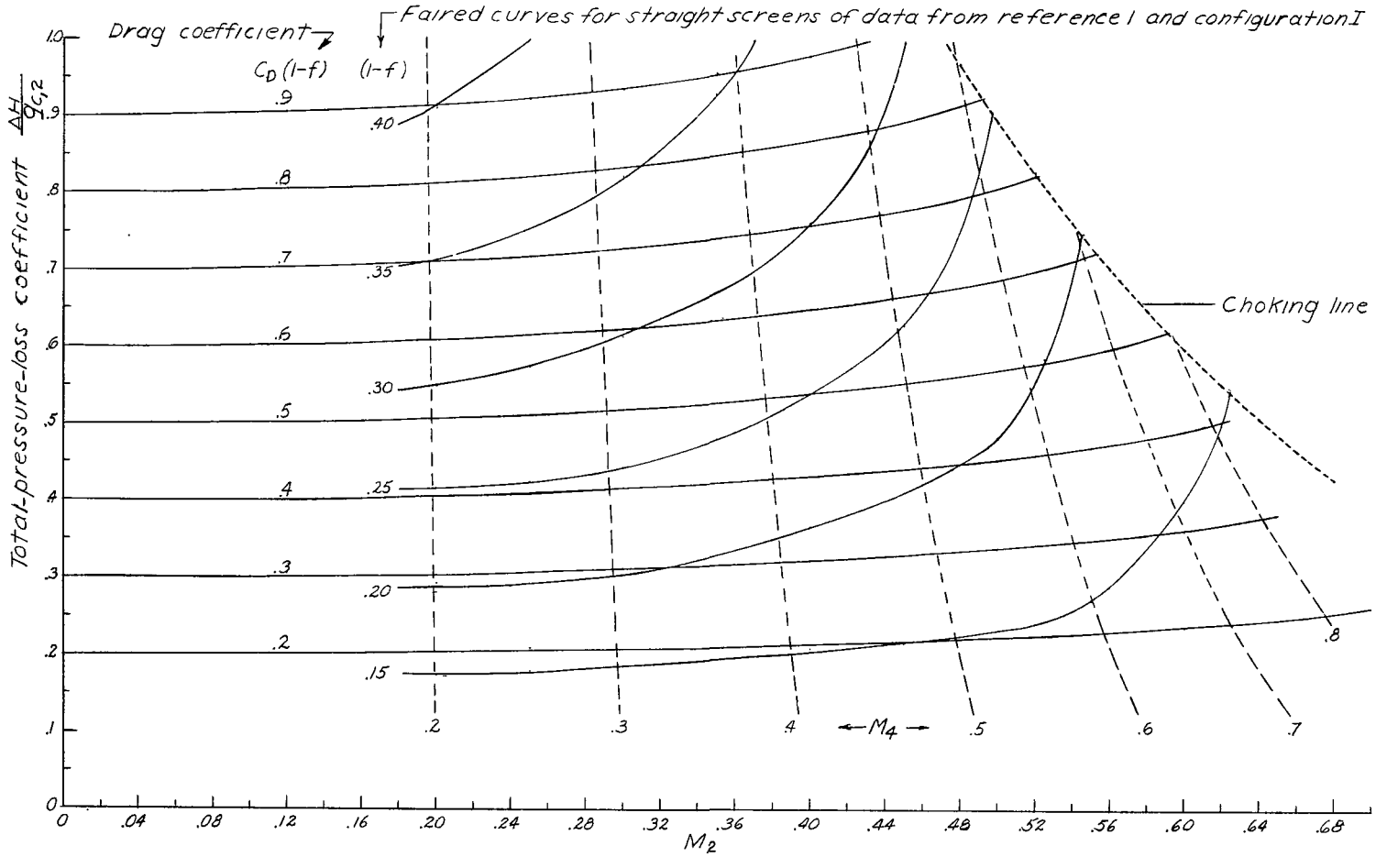

Figure 19.- Total-pressure-loss coefficient design chart for straight screens for values of loss coefficient from 0 to 1.0.

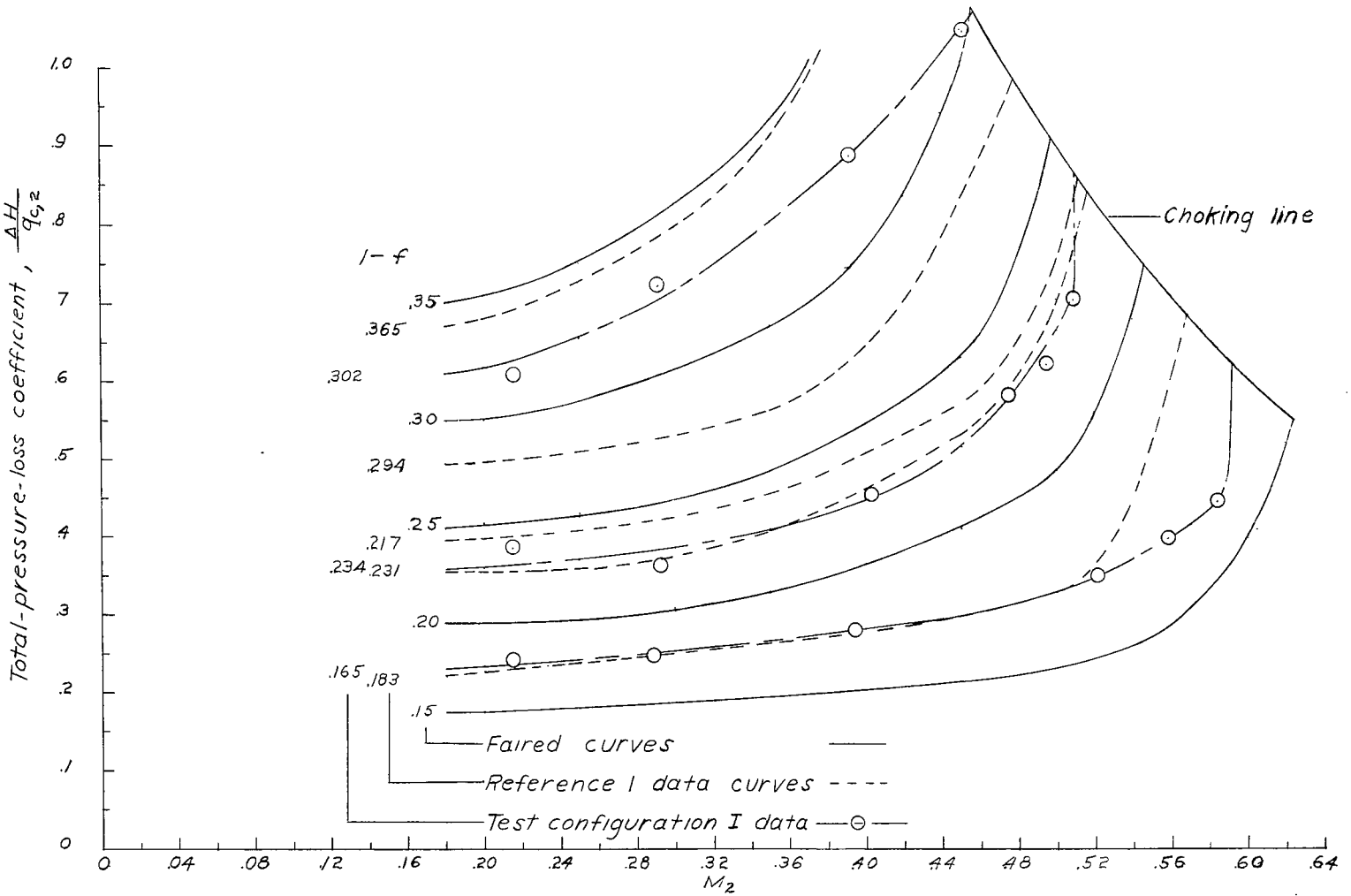

Figure 20.- Comparison of original data on total-pressure-loss coefficient for straight screens with faired curves.

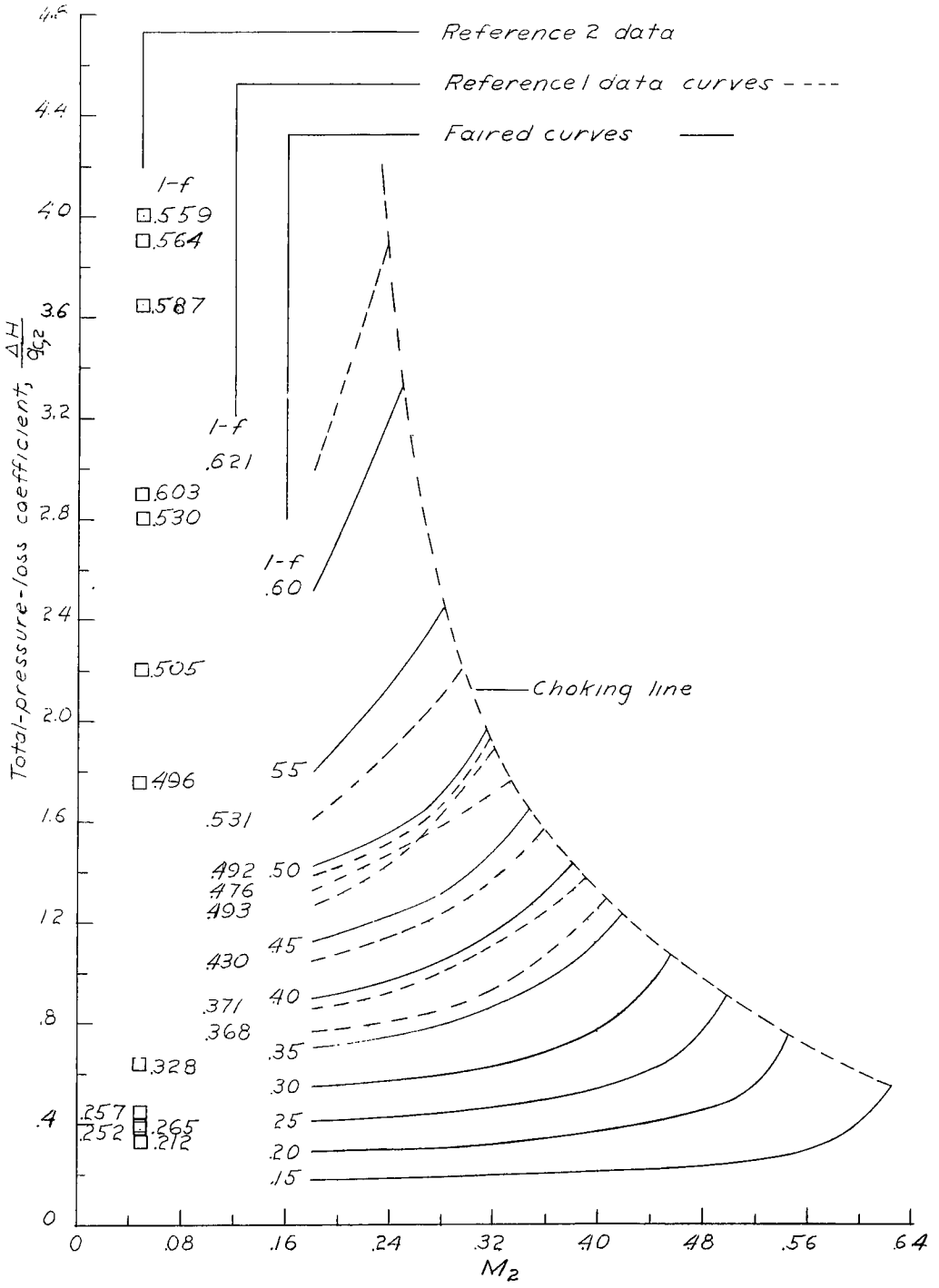

Figure 21.- Comparison of original data on total-pressure-loss coefficient for straight screen from references 1 and 2 with faired curves.

[redacted]

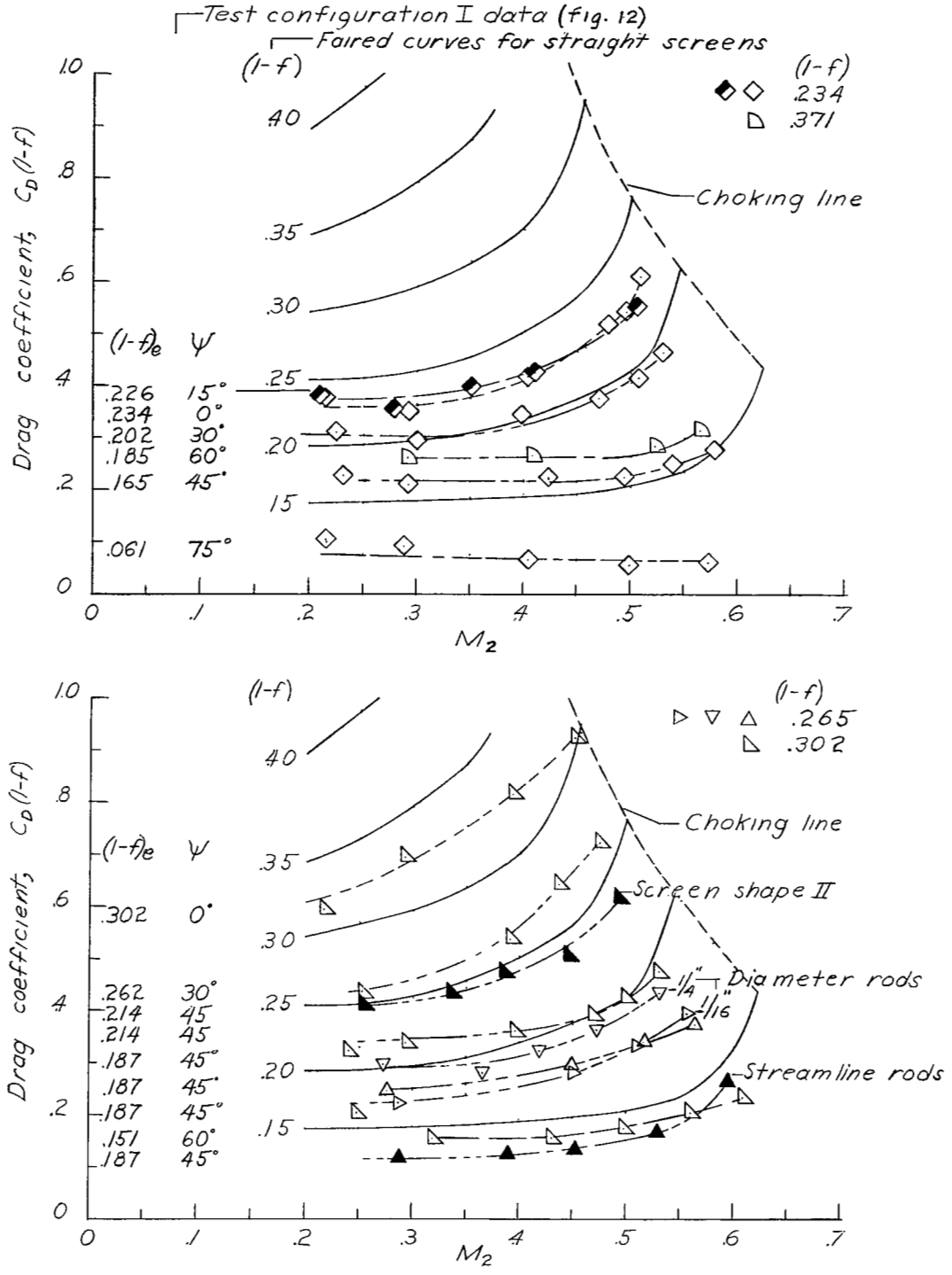

Figure 22.- Comparison of drag-coefficient data for configuration I with faired curves for straight screens.

[redacted]

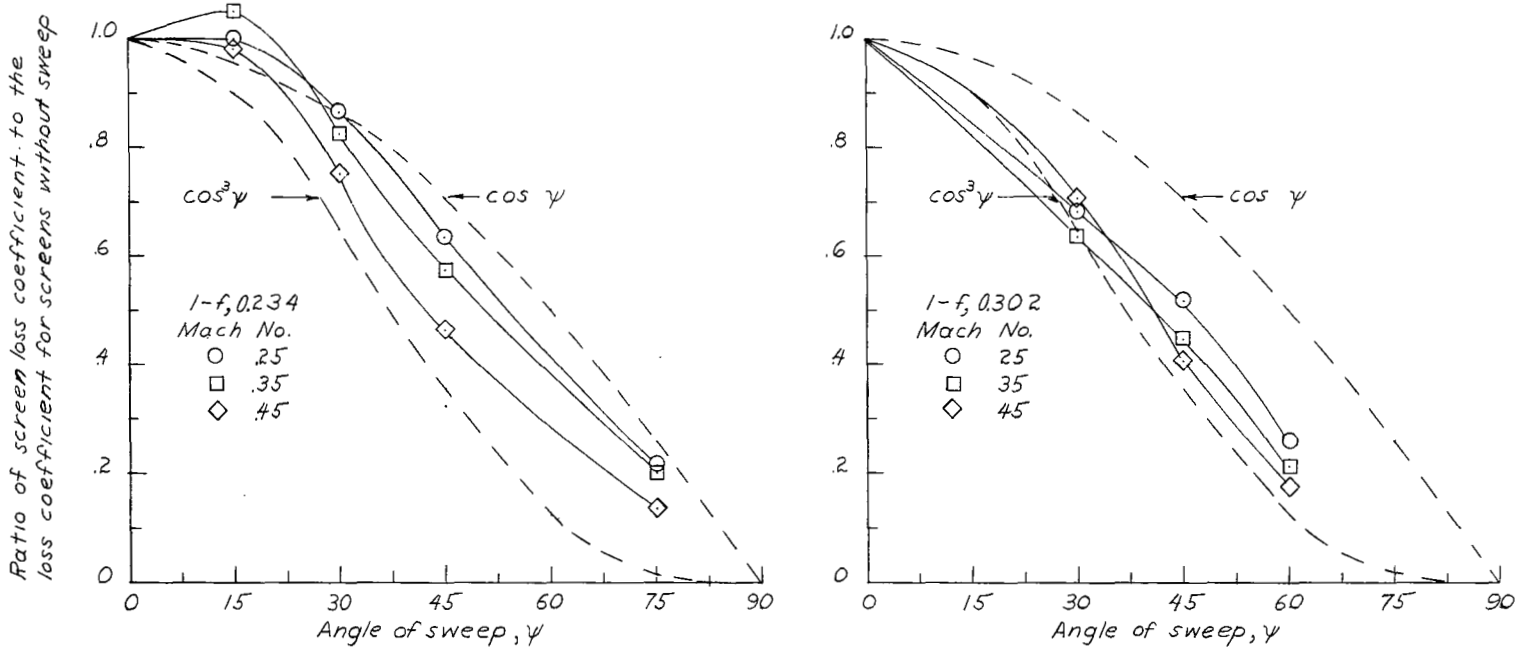

Figure 23.- Effect of screen sweep angle on total-pressure loss of screens. Configuration I.

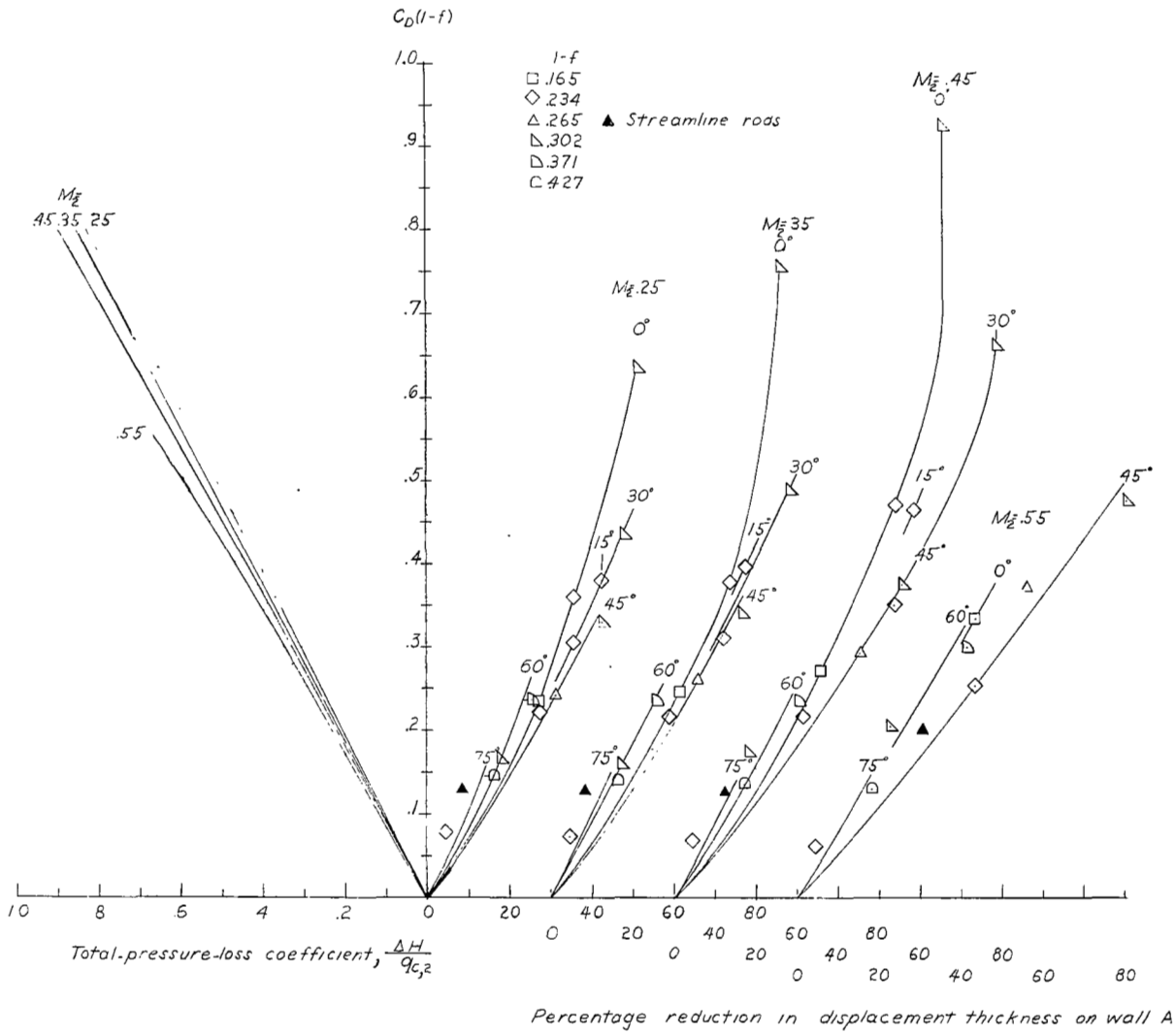

Figure 24.- Drag coefficient as a function of loss coefficient and percentage reduction in displacement thickness for the screens tested. Configuration I.

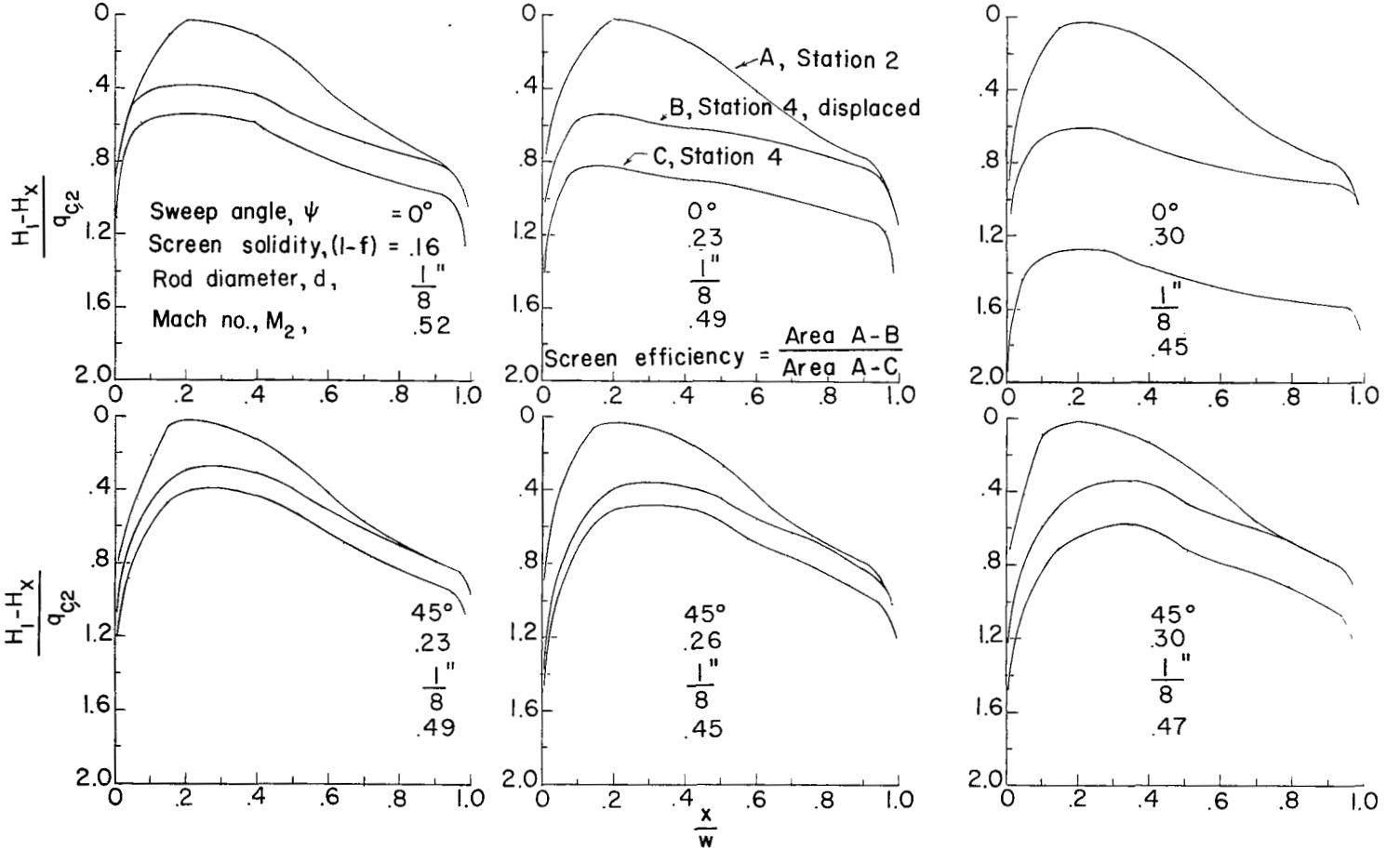

Figure 25.- Typical effects of screens on the total-pressure distribution. Configuration I.

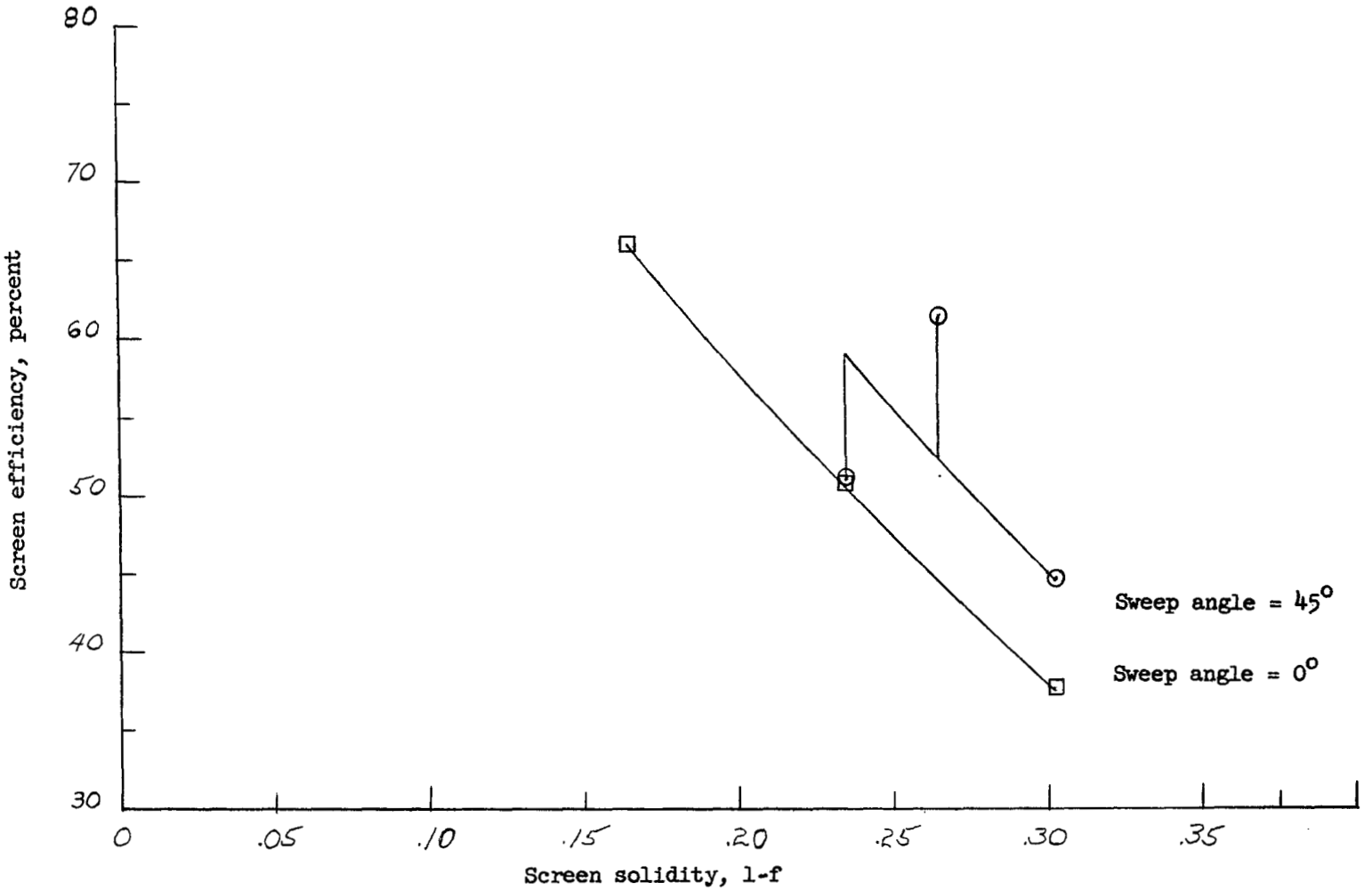

Figure 26.- Variation of screen efficiency with screen solidity. Test configuration II.

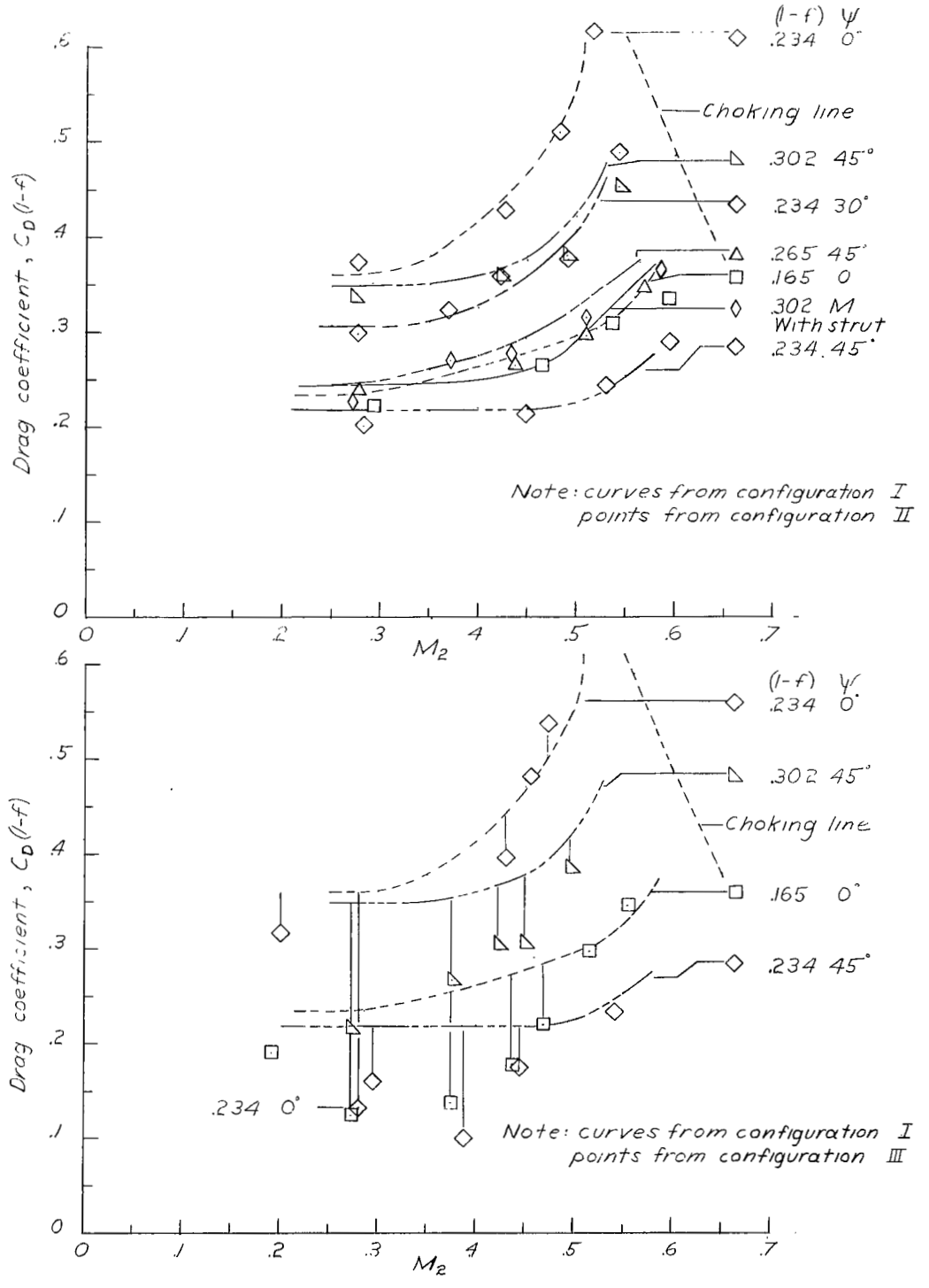

Figure 27.- Comparison of the drag coefficient for configurations I, II, and III.

[redacted]

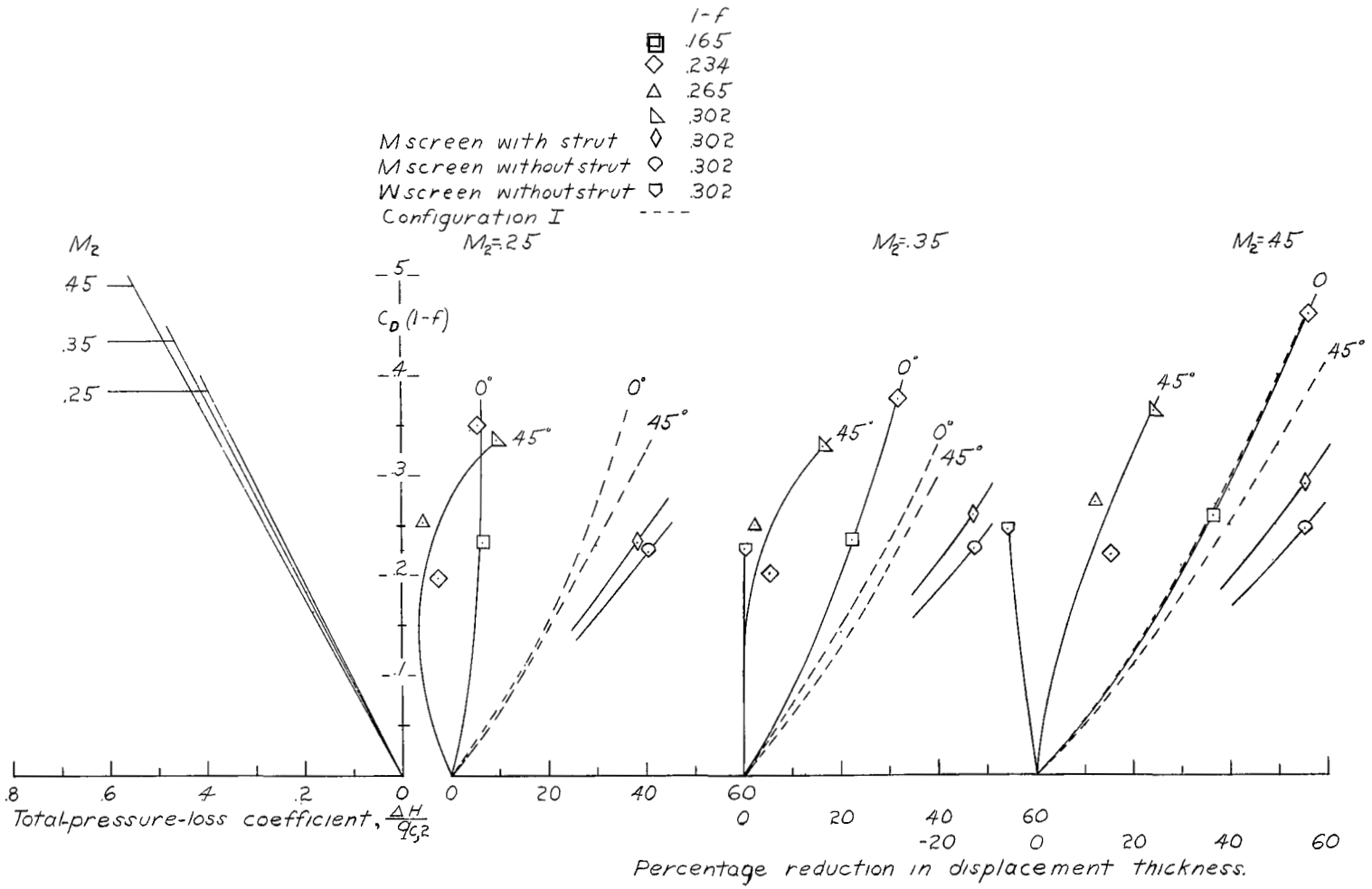

Figure 28.- Drag coefficient as a function of total-pressure-loss coefficient and percentage reduction in displacement thickness for the screens tested. Configuration II.

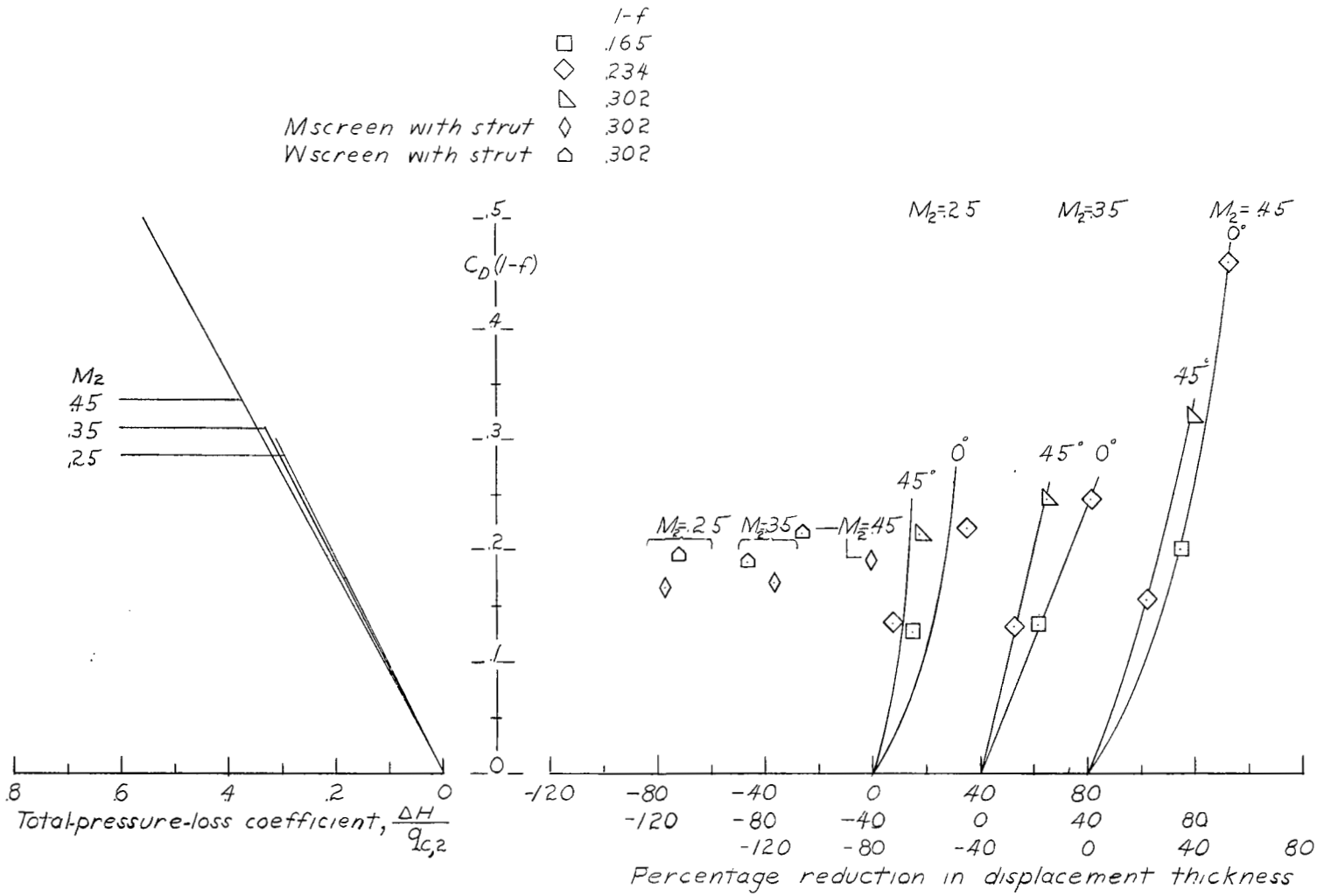

Figure 29.- Drag coefficient as a function of total-pressure-loss coefficient and percentage reduction in displacement thickness for the screens tested. Configuration III.

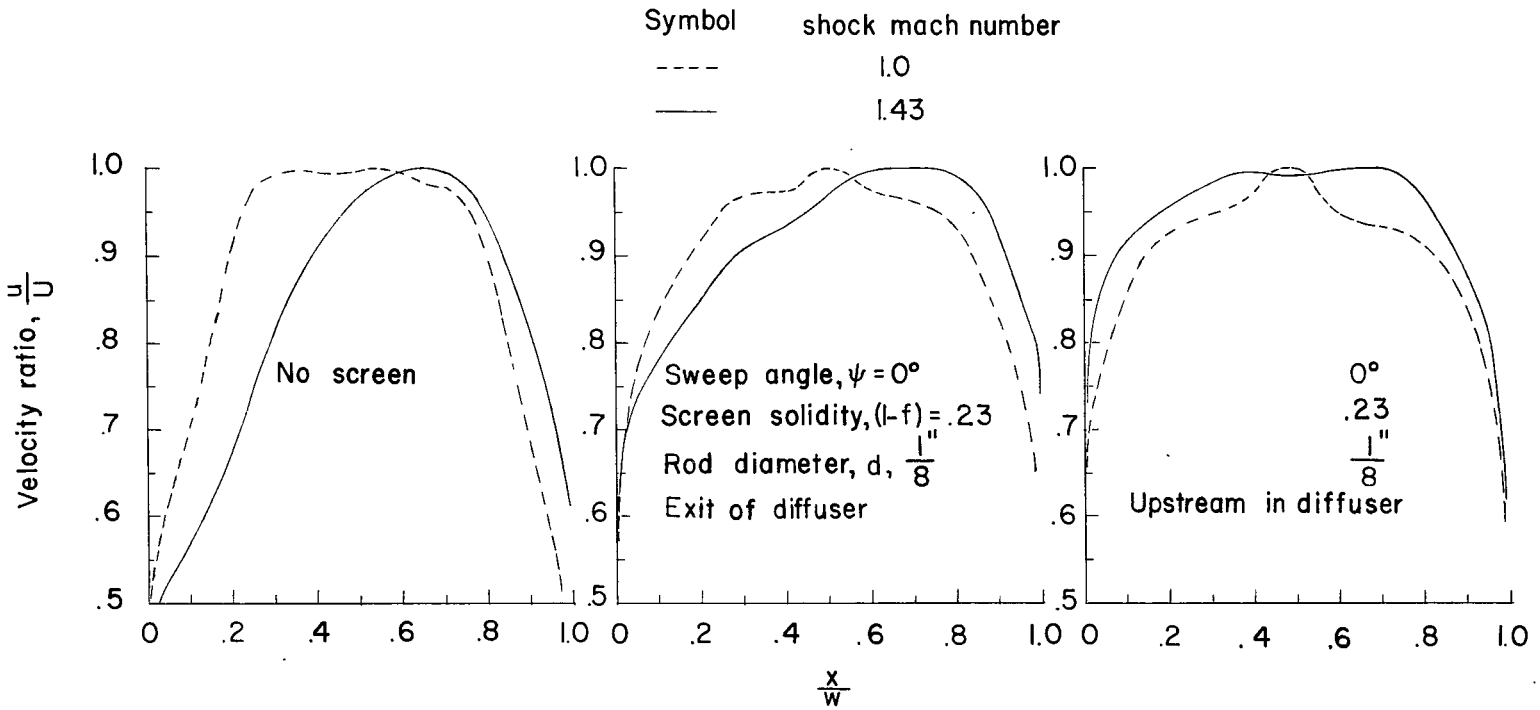

(a) No screen and straight screens.

Figure 30.- Velocity distributions at station 4 for a diffuser with screens located at the diffuser exit and upstream in the diffuser. Measurements presented are in the plane of the major flow distortion.

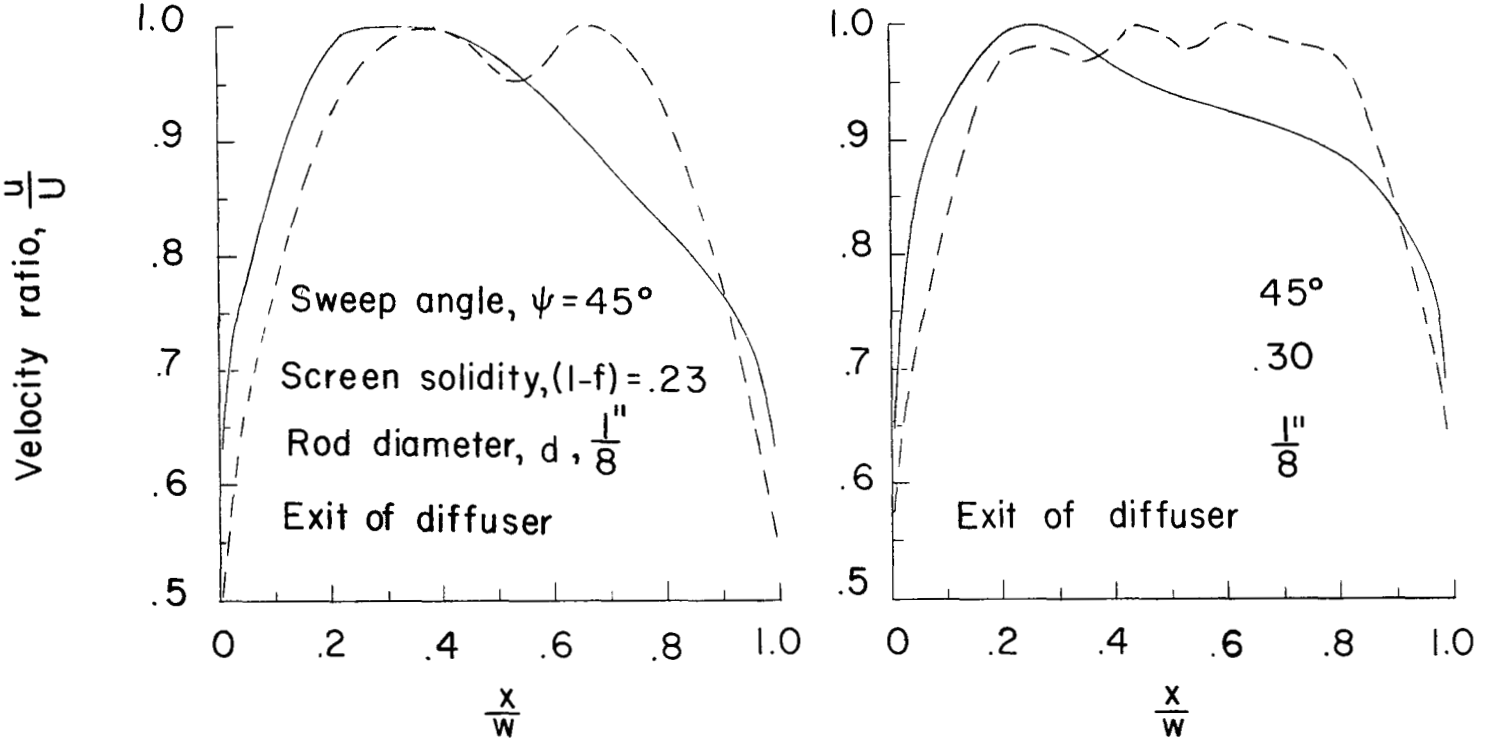

(b) Swept screens.

Figure 30.- Concluded.

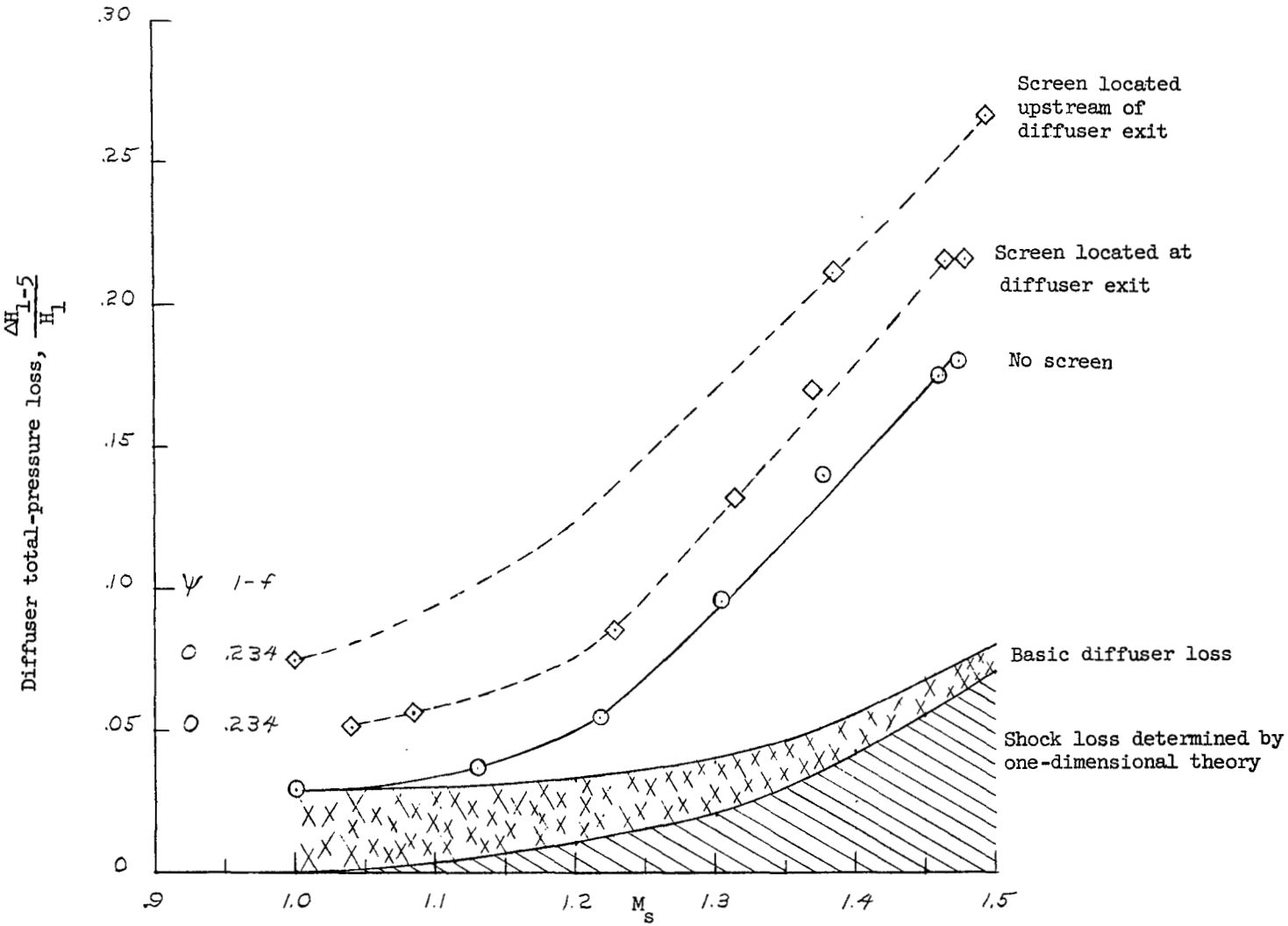

Figure 31.- Diffuser total-pressure loss without screens and for two different screen installations as a function of shock Mach number in the diffuser.

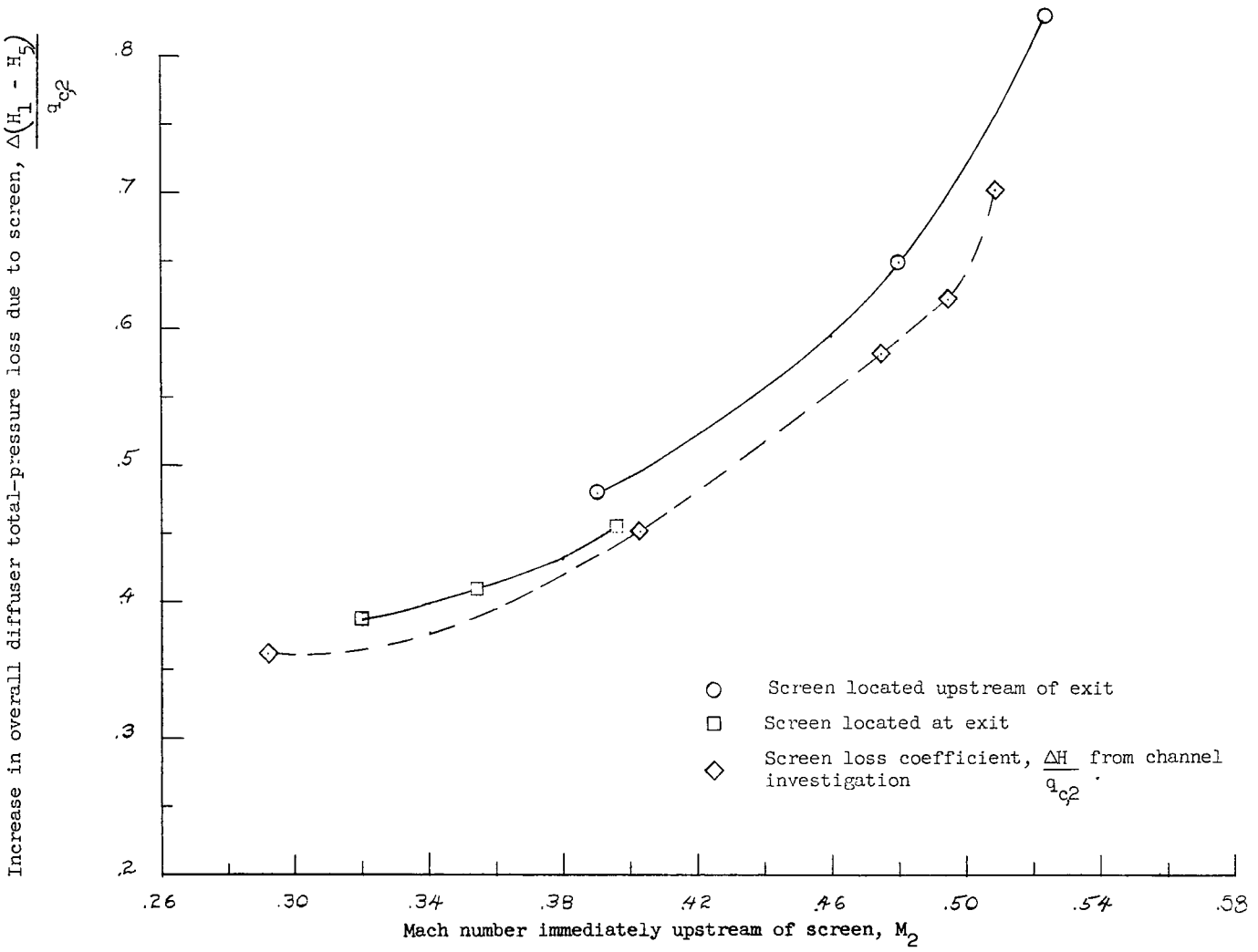

Figure 32.- Changes in the diffuser total-pressure-loss characteristics resulting from two different screen installations.